The Aryl Hydrocarbon Receptor Regulates Epidermal Differentiation through Transient Activation of TFAP2A

Jos P.H. Smits[1,2,5], Jieqiong Qu[3,5], Felicitas Pardow[1,3,6], Noa J.M. van den Brink[1,6], Diana Rodijk-Olthuis[1], Ivonne M.J.J. van Vlijmen-Willems[1], Simon J. van Heeringen[3], Patrick L.J.M. Zeeuwen[1], Joost Schalkwijk[1], Huiqing Zhou[3,4] and Ellen H. van den Bogaard[1]

The aryl hydrocarbon receptor (AHR) is an evolutionary conserved environmental sensor identified as an indispensable regulator of epithelial homeostasis and barrier organ function. Molecular signaling cascade and target genes upon AHR activation and their contribution to cell and tissue function are however not fully understood. Multiomics analyses using human skin keratinocytes revealed that upon ligand activation, AHR binds open chromatin to induce expression of transcription factors, for example, TFAP2A, as a swift response to environmental stimuli. The terminal differentiation program, including upregulation of barrier genes, *FLG* and keratins, was mediated by TFAP2A as a secondary response to AHR activation. The role of AHR–TFAP2A axis in controlling keratinocyte terminal differentiation for proper barrier formation was further confirmed using CRISPR/Cas9 in human epidermal equivalents. Overall, the study provides additional insights into the molecular mechanism behind AHR-mediated barrier function and identifies potential targets for the treatment of skin barrier diseases.

Keywords: AHR, coal tar, epithelium development, TCDD, TFAP2A

Journal of Investigative Dermatology (2024) **144,** 2013–2028; doi:10.1016/j.jid.2024.01.030

INTRODUCTION

The skin, being an important barrier organ, plays a major role in protecting and fostering the life it encloses. Within the ever-renewing epidermis, keratinocytes are the predominant cell type, accounting for 95% of epidermal cells (Freinkel and Woodley, 2001). The continuous renewing of the epidermis is highly dependent on the delicate balance between keratinocyte proliferation and differentiation. During epidermal development, basal stem cells give rise to daughter cells that undergo a coordinated program of cell cycle arrest, upward migration, and terminal differentiation. Maintaining the integrity of the epidermis is essential for skin homeostasis and protection of the host against infections, allergens, UVR, and other external threats through host defense and physical, chemical, and immunological barrier mechanisms (Nestle et al, 2009). As such, a compromised epidermal barrier is a prominent feature of common inflammatory skin diseases, such as atopic dermatitis and psoriasis (Angelova-Fischer et al, 2011; Nomura et al, 2003). In healthy skin, epidermal homeostasis is tightly controlled through a set of essential transcription factors (TFs), for example, TP63, AP1, and the aryl hydrocarbon receptor (AHR) (Candi et al, 2008; Eckert et al, 2013; Esser et al, 2013).

AHR is a TF that is considered a sensor of environmental, microbial, metabolic, and endogenous cues. Depending on the specific activating ligand, AHR activation can cascade into a response ranging from highly toxic to therapeutic (Denison and Nagy, 2003; Esser et al, 2013; Rothhammer and Quintana, 2019). AHR is involved in many biological processes, from cellular proliferation and differentiation to immune responses both innate and adaptive origin. Upon activation, AHR translocates from the cytoplasm to the nucleus, where it dimerizes with AHR nuclear transporter to bind to its cognate DNA consensus sequence (5′-TNGCGTG-3′) known as the xenobiotic response element and regulates gene transcription (Esser et al, 2013; Yao and Denison, 1992). Certain AHR-activating ligands are highly toxic, for example, high-affinity environmental pollutant dioxins (eg, 2,3,7,8-Tetrachlorodibenzo-*p*-dioxin [TCDD]). TCDD has an extremely long half-life (estimated at 7.1 years in humans), resulting in prolonged and uncontrolled AHR activation

[1]*Department of Dermatology, Radboud Research Institute for Medical Innovation, Radboudumc, Nijmegen, The Netherlands;* [2]*Department of Dermatology, University Hospital Düsseldorf, Medical Faculty, Heinrich Heine University, Düsseldorf, Germany;* [3]*Department of Molecular Developmental Biology, Faculty of Science, Radboud University, Nijmegen, The Netherlands; and* [4]*Department of Human Genetics, Radboudumc, Nijmegen, The Netherlands*

[5]*These authors contributed equally to this work.*

[6]*These authors contributed equally to this work.*

Correspondence: Ellen H. Van den Bogaard, Department of Dermatology, Radboud Research Institute for Medical Innovation, Radboudumc, Nijmegen, The Netherlands. E-mail: Ellen.vandenBogaard@radboudumc.nl and Huiqing Zhou, Department of Molecular Developmental Biology, Faculty of Science, Radboud University, Nijmegen, The Netherlands. E-mail: j.zhou@science.ru.nl; jo.zhou@radboudumc.nl

Abbreviations: AHR, aryl hydrocarbon receptor; C2, cluster 2; ChIP, chromatin immunoprecipitation; CT, coal tar; DEG, differentially expressed gene; EIS, electrical impedance spectroscopy; ERG, early-responsive gene; GO, gene ontology; HEE, human epidermal equivalent; IVL, involucrin; LRG, late-responsive gene; siRNA, small interfering RNA; TCDD, 2,3,7,8-tetrachlorodibenzo-p-dioxin; TEWL, transepidermal water loss; TF, transcription factor

Received 7 September 2023; revised 29 January 2024; accepted 31 January 2024; Accepted manuscript published online 22 February 2024; corrected proof published online 24 May 2024

(Pirkle et al, 1989; Ray and Swanson, 2004), whereas other AHR ligands are rapidly degraded and considered of more physiological importance, for example, 6-formylindolo[3,2-b]carbazole, which is generated upon UVR of keratinocytes (Fritsche et al, 2007; Rannug et al, 1995, 1987).

Over the years, we have gained a better understanding of the effects of AHR activation on inflammatory skin conditions since the discovery of AHR activation as the working mechanism of coal tar (CT) ointment that was used for psoriasis and atopic dermatitis treatment (McLean and Irvine, 2013; Smits et al, 2020; van den Bogaard Ellen et al, 2013). These insights sparked the global interest in therapeutics that target the AHR in skin diseases and beyond and led to the registration of Tapinarof, an AHR ligand, for psoriasis (Peppers et al, 2019; Smith et al, 2017b). Phase 3 clinical trials in atopic dermatitis are ongoing (NCT05032859). Other AHR ligands with similar biological implications, including carboxamide and indazole derivatives, have also been studied for their therapeutic anti-inflammatory and barrier-promoting potential (Kaye et al, 2016; Nilsson et al, 1995; Rikken et al, 2023, 2022; Wegner et al, 2010).

At the molecular level, mainly 4 groups of genes are known to be targeted by AHR in the skin: first, a battery of xenobiotic metabolizing enzymes, including cytochrome P450 monooxygenases (P450s), for example, *CYP1A1* (Ramadoss and Perdew, 2005); second, genes involved in keratinocytes differentiation (Loertscher et al, 2001), for example, *FLG* and involucrin (IVL) gene *IVL* (Hidaka et al, 2017; Sutter et al, 2011; Tsuji et al, 2017; van den Bogaard Ellen et al, 2013); third, genes related to host defense, for example, the antimicrobial peptide families of *S100* genes, late cornified envelope genes, and *PI3*, among others (Smits et al, 2020; Sutter et al, 2011); and finally, genes related to immunity, for example, the inflammatory cytokines *IL1β*, *IL6*, *CXCL5*, *CCL20*, and *IL10* (Hollingshead et al, 2008; Smith et al, 2017a; Vogel et al, 2016). Hence, AHR activation is found to increase epidermal differentiation and barrier formation (Furue et al, 2015; Sutter et al, 2011; van den Bogaard et al, 2015, 2013) and dampen skin inflammation (Di Meglio et al, 2014). However, the sequence and dynamics of the molecular events and other players involved through which AHR mediates these effects are poorly understood.

In this study, we aim to characterize regulatory cascade upon AHR activation in human keratinocytes. Through transcriptomic and epigenomic analyses, we identified a hitherto unrecognized AHR—TFAP2A axis that regulates epidermal keratinocyte terminal differentiation and skin barrier formation.

RESULTS

AHR activation results in distinct early and late transcriptional programs

To characterize the gene expression pattern upon AHR activation in human primary keratinocytes, we performed RNA sequencing on keratinocytes either treated with TCDD or CT, 2 AHR model ligands, for short-term (2 hours) and longer-exposure (24 hours) duration. Principle component analysis showed transcriptome alterations in ligand-treated samples already after 2 hours of treatment, indicating that ligand exposure results in swift AHR activation and transcription regulation (Figure 1a). The differences became increasingly apparent between 2 hours and 24 hours of ligand treatment, indicated as the major change through principal component 1 axis (71% variance). Differences between TCDD- and CT-treated samples were minor because they closely clustered in the principle component analysis plot, indicating that regulatory events downstream of AHR activation are similar in both treatment conditions. *CYP1A1* and *CYP1B1*, target genes in canonical AHR signaling, showed consistent upregulation upon both ligand treatments, more significantly after 24-hour treatment (Figure 1b). Their gene expression was validated with qPCR (Figure 1c). These observations indicate that TCDD and CT treatment activate AHR signaling pathways through a similar pool of genes within 24 hours, and we therefore focused on the common mechanism shared between TCDD and CT treatment in subsequent analyses, referred to as ligand treatment in the remaining parts of this paper.

Next, we identified differentially expressed genes (DEGs) (adjusted $P < .05$) between the control and at both 2 hours and 24 hours of ligand treatment. In total, 8160 DEGs were grouped into 8 hierarchical clusters according to the gene expression dynamics at different time points after ligand treatment (Figure 1d and Table 1 and Supplementary Data S1). Clusters 1 and 2 show early downregulation upon ligand treatment, with no apparent late effects or dampened downregulation after 24 hours of treatment, respectively. Cluster 3 and cluster 8 comprised the majority of DEGs, but their gene expression was unrelated to AHR ligand treatment and was mainly affected by the keratinocyte differentiation itself. Genes from cluster 3 are mainly associated with gene ontology (GO) term cell cycle, and genes from cluster 8 are involved in translation. Importantly, genes in cluster 4 showed upregulated expression after 2-hour ligand treatment and are involved in the processes of phosphorylation and epithelium development, for example, *NOTCH2*, *JUN*, *TFAP2A*, keratin 4 gene *K4*, and *POU3F1*. In contrast, genes in cluster 5 showed late upregulated expression only after 24 hours of ligand treatment and mainly contribute to keratinocyte differentiation, for example, *FLG* and *IVL*, and oxidation—reduction process, for example, *HYAL1* and *CYCS*. Cluster 6 contains genes that are slightly upregulated early after ligand treatment. These genes appear downregulated at 24 hours in control, probably owing to differentiation, whereas ligand treatment at this time point dampens the downregulation. Cluster 7 contains genes that are downregulated 24 hours after treatment initiation. Interestingly, there was no distinct cluster of genes that showed continuous upregulation or downregulation 2 and 24 hours after TCDD and CT treatment. This highlights the dynamics of AHR signaling in primary cells rather than the reported continuous signaling in (cancer) cell lines (Wang et al, 2020).

To dissect the molecular events upon AHR activation, we continued to focus on clusters of early-responsive genes (ERGs) (cluster 4) (Figure 1e) (upregulation 2 hours after ligand treatment) and late-responsive genes (LRGs) (cluster 5) (Figure 1f) (upregulation 24 hours after ligand treatment). The separation of ERGs and LRGs suggests a different regulatory mechanism of AHR signaling between early and late responses. This observation led us to hypothesize that the early and late responses are potentially linked through TFs in ERGs that activate transcription of LRGs. Indeed, among the 8160

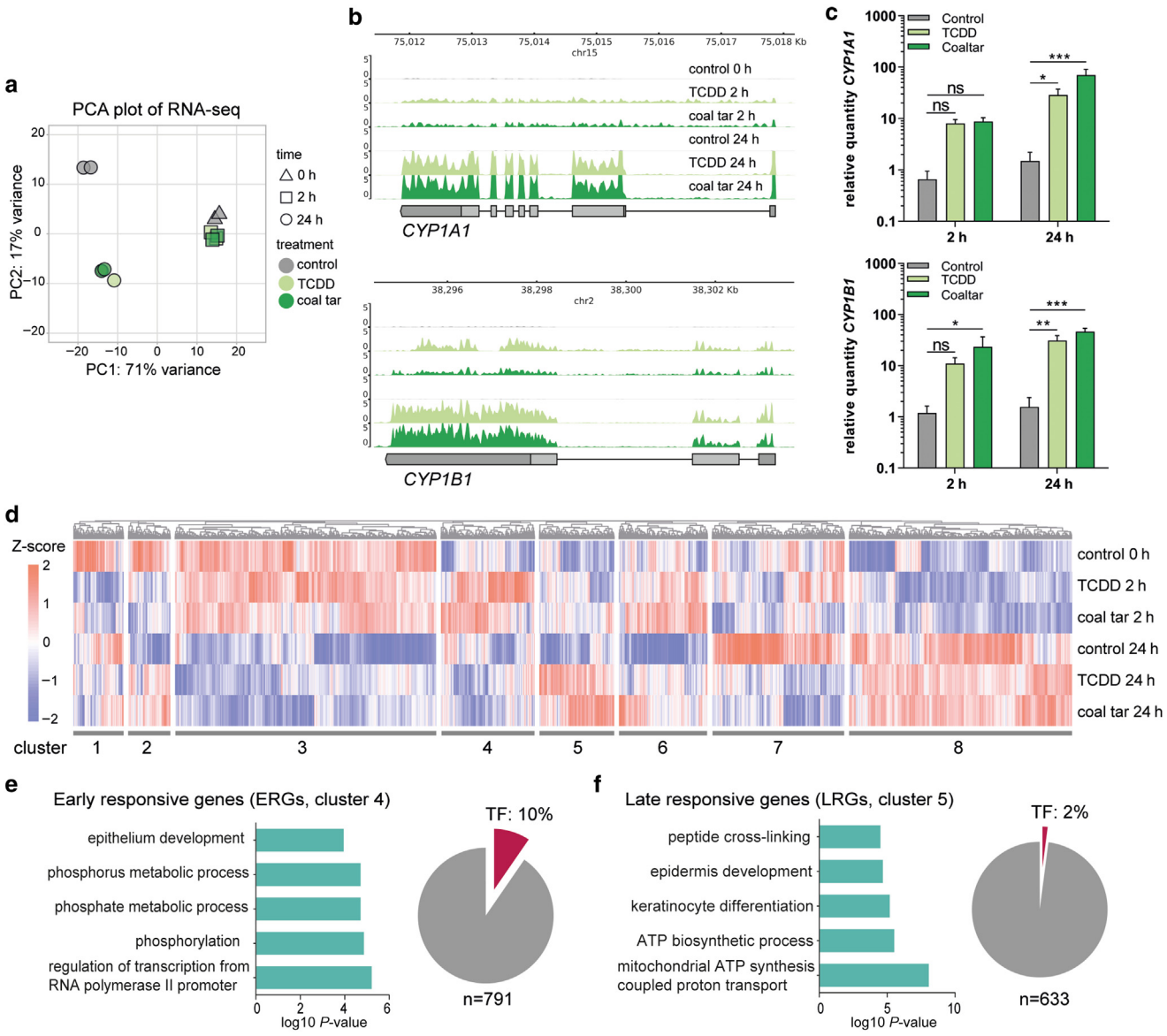

Figure 1. AHR activation results in distinct early and late response. (**a**) PCA of RNA-seq data indicating that 24 h after TCDD or coal tar treatment, the response is highly similar. (**b**) Genome browser screenshots of *CYP1A1* and *CYP1B1* on RNA-seq tracks. (**c**) RT-qPCR validation of *CYP1A1* and *CYP1B1*. Data are shown as mean ± SEM, n = 5 technical replicates, 2-way ANOVA, ns $P > .05$, *$P < .05$, **$P < .01$, and ***$P < .001$. (**d**) Hierarchical clustering of differentially expressed genes ($P < .05$). Z-score was calculated on the basis of log10 (FPKM + 0.01) of each gene. (**e**) GO annotation of ERGs, accompanied by a pie chart showing the number and percentage of TFs within the (**f**) GO annotation of LRGs, accompanied by a pie chart showing the number and percentage of TFs within the cluster. AHR, aryl hydrocarbon receptor; ERG, early-responsive gene; FPKM, fragments per kilobase of transcript per million mapped reads; GO, gene ontology; h, hour; LRG, late-responsive gene; ns, sonsignificant; PC, principal component; PCA, principal component analysis; RNA-seq, RNA sequencing; TCDD, 2,3,7,8-tetrachlorodibenzo-p-dioxin; TF, transcription factor.

DEGs, 558 genes were classified as TFs, and 76 TFs of 791 genes (10%, hypergeometric $P = .001$) were found in ERGs, for example, *HES1*, *HES2*, *FOSL1*, *JUN*, *TFAP2A*, and *SOX4*. In contrast, LRGs did not show significant enrichment of TFs (13 TFs in 633 genes, eg, *GRHL1* and ignal transducer and activator of transcription 6 gene *STAT6*; hypergeometric $P =$ 1.2) (Figure 1e and f and Supplementary Data S1). This clear enrichment of TFs in ERGs in contrast to that in LRGs supports our hypothesis that the upregulated TFs among ERGs regulated the expression of LRGs, including the expression of epidermal differentiation genes.

AHR activation promotes dynamic alterations of the enhancer landscape

To identify AHR-target genes, including TFs, we set out to first map enhancers bound by AHR. Being a receptor of environmental cues, AHR was expected to bind to chromatin in a swift and transient manner, and therefore, we first performed AHR-targeted chromatin immunoprecipitation (ChIP) followed by qPCR to determine the binding time frame. At 30 minutes of ligand treatment, AHR-binding signals were detected at the loci of the known AHR-target gene *CYP1A2* (Figure 2a). Such fast binding of AHR was consistent with the

Table 1. Hierarchical Clusters with Significantly DE Genes of Ligand-Treated Keratinocytes

Cluster	Cluster Size	Gene Expression Dynamics upon AHR Ligand Treatment	Most Significant GO Term	Example Genes
1	425 genes	Early (downregulated) responsive, with no apparent late effects	GO:0070647 protein modification by small protein conjugation or removal	*BBS2, KIF3A*
2	355 genes	Early (downregulated) responsive. Genes appear downregulated in 24-hour control, whereas ligand treatment dampens this downregulation	GO:0051301 cell division	*CDK1*
3	2207 genes	Nonresponsive to treatment	GO:0007049 cell cycle	*E2F1*
4	791 genes	Early (upregulated) responsive (ERGs)	GO:0060429 epithelium development	*NOTCH2, JUN, TFAP2A, K4, POU3F1*
5	633 genes	Late (upregulated) responsive (LRGs)	GO:0008544 epidermis development	*FLG, IVL*
6	748 genes	Early (slightly upregulated) responsive. Genes appear downregulated in 24-hour control, whereas ligand treatment dampens this downregulation	GO:0007049 cell cycle	*HIST1H4L, POLR2F*
7	1118 genes	Late (downregulated) responsive genes	GO:0051252 regulation of RNA metabolic process	*HKR1, FOXO3, TGFB2*
8	1883 genes	Nonresponsive to treatment	GO:0002181 cytoplasmic translation	*RPL18*

Abbreviations: AHR, aryl hydrocarbon receptor; DE, differentially expressed; ERG, early-responsive gene; GO, gene ontology; IVL, involucrin; K4, keratin 4; LRG, late-responsive gene.

translocation of AHR from the cytoplasm to the nucleus as shown by immunofluorescent staining after 30 minutes of ligand treatment (Figure 2b). Notably, the AHR-binding signals decreased after 90 minutes of ligand treatment (Figure 2a), confirming the transient character of AHR interaction with its target loci. The dynamic binding on the genome by AHR in primary keratinocytes is consistent with our observations on gene expression changes upon AHR activation (Figure 1d).

Because we consistently observed similar gene expression and AHR binding after both TCDD and CT treatments, we continued our experiments with only TCDD stimulation to model AHR activation. To identify AHR-responsive enhancers that are involved in gene activation, we performed H3K27ac ChIP sequencing after TCDD treatment for 30 and 90 minutes. Clustering of enhancer regions based on H3K27ac signals gave rise to 4 clusters consisting of 4604 enhancers (Figure 2c and Supplementary Data S2). Subsequently, motif analysis was performed to predict TFs that potentially bind to these enhancers (Figure 2e and Supplementary Data S2). Among the 4 clusters, only cluster 1 (shown as C1) containing a small number (186) of enhancer regions showed decreased activity upon AHR activation by TCDD at 30 minutes (Figure 2c), and motif analysis did not yield statistically enriched TF motifs (Supplementary Data S2). Cluster 2 (C2) represents 945 enhancer regions that showed a reasonable level of H3K27ac signals in the control (0 minutes) and increased signals at 30 minutes of TCDD treatment. The H3K27ac signals remained high after 90 minutes. Genes nearby these enhancers are mainly involved in omega-hydroxylase P450 pathway shown by the GO analysis (Figure 2d) and contain many known AHR targets, such as *CYP1A1* and *CYP1A2*. TF motif analysis showed that the AHR motif was the only highly enriched motif in C2, indicating that this cluster of enhancers is likely directly bound by AHR (Figure 2e and Supplementary Data S2). Cluster 3 contains 2470 enhancer regions maintaining high signals at 0 and 30 minutes, which decreased after 90 minutes of TCDD treatment. Genes near these enhancers are mainly involved in the regulation of Notch signaling pathway, for example, *BMP7*, *HES1*, *JAG1*, and immune system development, for example, *BCL6* and *CD28* (Figure 2d). CHOP-, ATF4-, AARE-, and CEBP-binding motifs from the activator protein-1 motif family were enriched in cluster 3 enhancers (Figure 2e and Supplementary Data S2). The last cluster, cluster 4, consisted of 1003 enhancers showing higher activity only after 90 minutes of TCDD treatment, with nearby genes being predominantly involved in keratinocyte differentiation, for example, *FLG* and *HRNR*. This cluster did not contain significantly enriched TF-binding motifs (Supplementary Data S2).

To confirm the motif analysis of C2 in which the AHR motif was enriched, we performed AHR ChIP sequencing with TCDD treatment and obtained 57 AHR-binding sites (adjusted $P = 1e\text{-}4$) (Supplementary Data S3). When examining H3K27ac signals at AHR-binding sites, we observed persistent H3K27ac signals at both 30 and 90 minutes of treatments (Figure 2f), fully consistent with C2 cluster enhancer signals (Figure 2c), confirming this cluster of enhancers to be direct targets of AHR. Of note, the apparent H3K27ac signals at most of the C2 enhancers in the control without ligands indicate that AHR binds to open chromatin regions. At the same time, AHR-binding signals peaked at 30 minutes and went down after 90 minutes of treatment (Figure 2g), in line with the transient AHR binding observed from ChIP followed by qPCR analysis of the CYP1A2 locus (Figure 2a).

In summary, these data demonstrate a transient nature of AHR-enhancer binding, leading to early activation of enhancer targets (C2) and the late activation of enhancers near epidermal differentiation genes (cluster 4). This distinct activation scheme is consistent with the temporal-divided expression pattern of ERGs and LRGs (Figure 1).

TFAP2A is direct target of AHR

To confirm our hypothesis that AHR-controlled TFs among ERGs regulate keratinocyte differentiation program as the secondary response to AHR activation and to identify such candidate TFs, we integrated the RNA-sequencing, AHR ChIP-sequencing, and H3K27ac ChIP-sequencing data. We

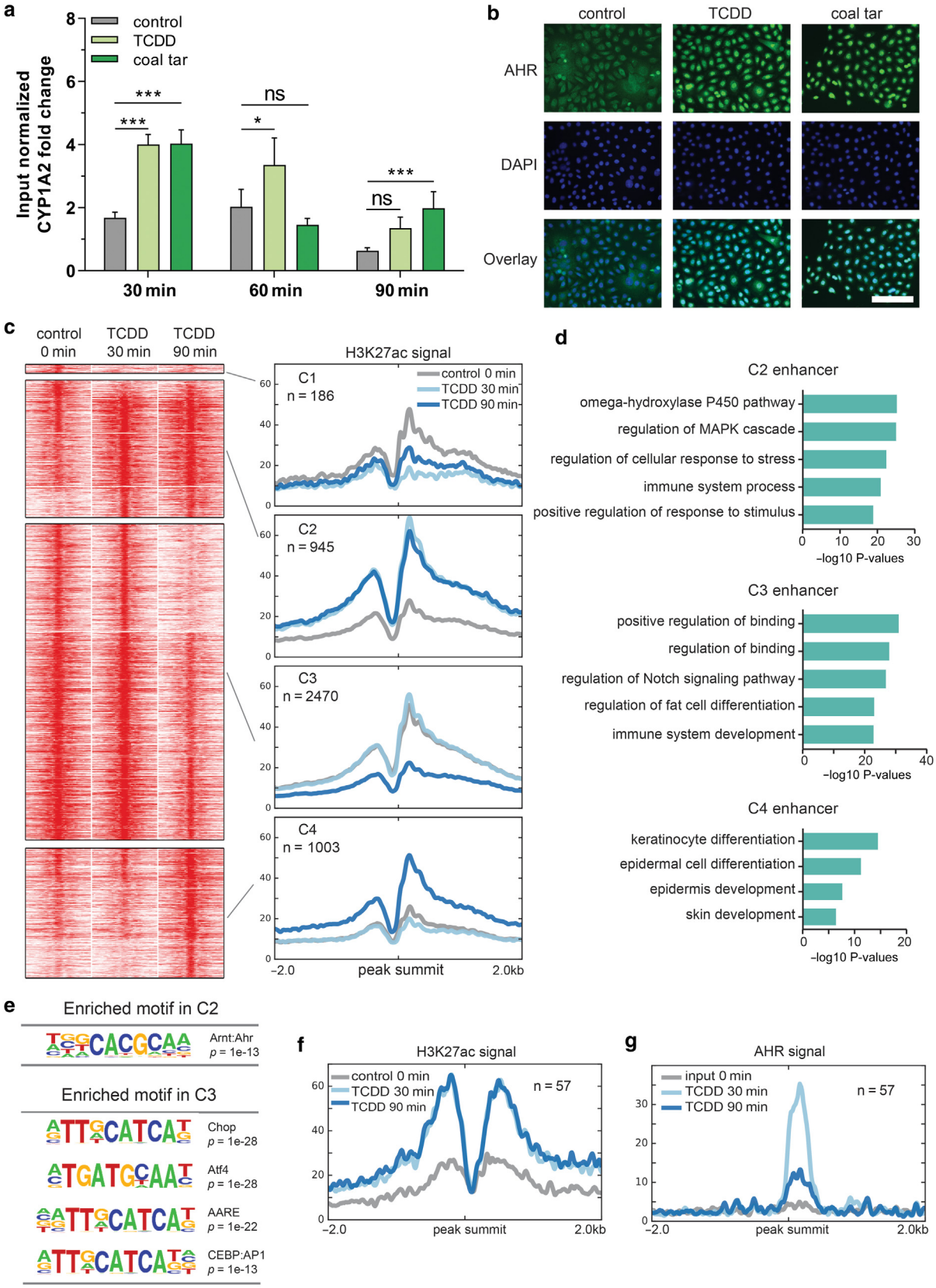

Figure 2. AHR activation leads to enhancer dynamics. (**a**) AHR ChIP RT-qPCR performed at the loci of *CYP1A2* (as a positive control) at different time point after ligand treatment. Input normalized fold change is relative to both input DNA and negative control loci (chr11). Data are shown as mean ± SEM, n = 6 technical replicates, 2-way ANOVA; ns, $P > .05$, $^{*}P < .05$, and $^{***}P < .001$. (**b**) AHR translocation from the cytoplasm to the nucleus after 30 min of ligand treatment. Bar = 100 μm. (**c**) Clustering of the dynamic enhancers upon AHR activation. Heat maps and band plots are shown in a 4-kb window with summits of enhancers in the middle. Color intensity in heat maps represents normalized read counts. In the band plots, the median enrichment was shown. (**d**) GO

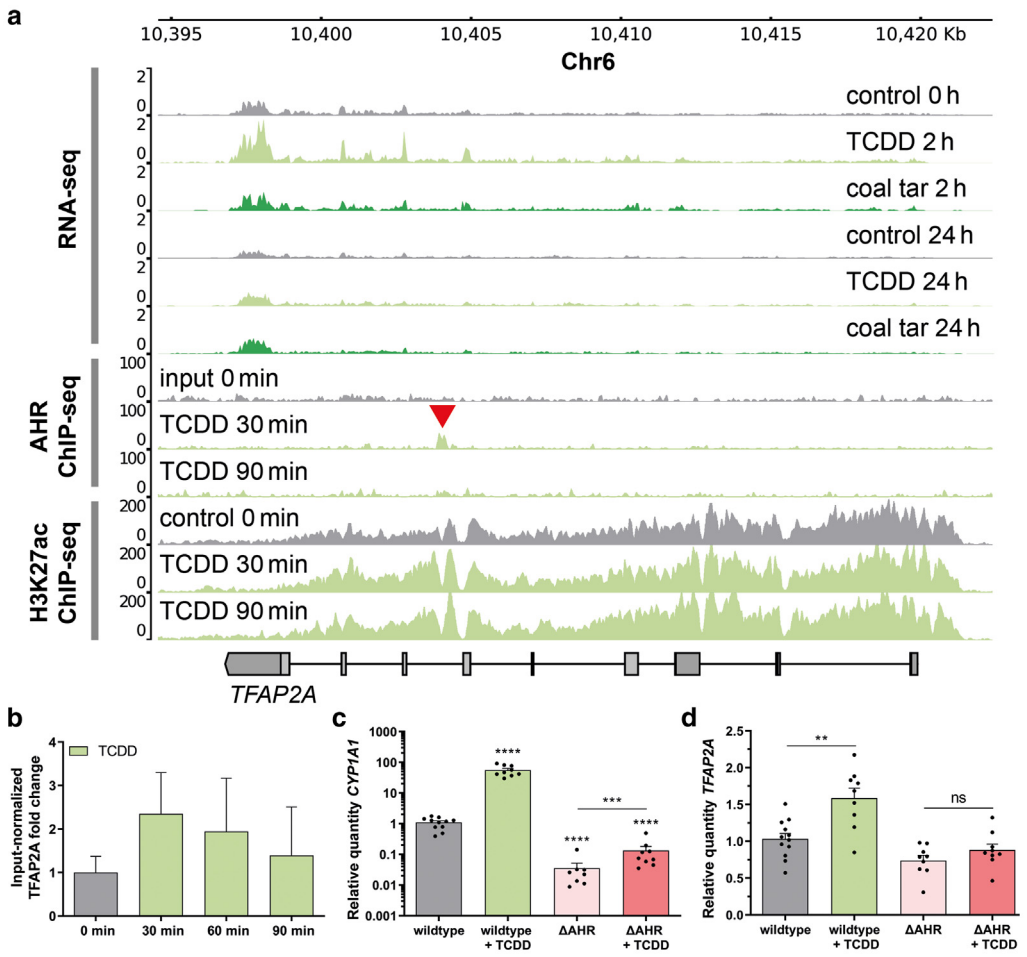

Figure 3. AHR targets TFAP2A in the early response to AHR ligands. (**a**) Genome browser screenshots of the *TFAP2A* coding region show RNA-seq, AHR ChIP-sequencing, and H3K27ac ChIP-sequencing tracks upon treatment with coal tar and TCDD. Red arrow indicates AHR-binding site within the *TFAP2A* locus. (**b**) AHR ChIP–RT-qPCR validation at the loci of *TFAP2A* at different time point after ligand treatment. Input-normalized fold change is relative to both input DNA and negative control loci (chr11). Data are shown as mean ± SEM, n = 2 technical replicates. (**c, d**) Knockout of AHR (ΔAHR) is accompanied by loss of *CYP1A1* (as classical AHR target) and *TFAP2A* expression. Data are shown as mean ± SEM, n > 5 technical replicates, 1-way ANOVA. ns, $P > .05$, $^{**}P < .01$, $^{***}P < .001$, and $^{****}P < .0001$. AHR, aryl hydrocarbon receptor; ChIP, chromatin immunoprecipitation; h, hour; min, minute; ns, sonsignificant; RNA-seq, RNA sequencing; TCDD, 2,3,7,8-tetrachlorodibenzo-p-dioxin; TF, transcription factor.

set the criteria of such intermediate TFs to exhibit upregulated gene expression upon AHR activation by ligands (cluster 4 in Figure 1d) and denoted by a nearby AHR-bound active enhancer as indicated by AHR and H3k27ac ChIP-sequencing signals. On the basis of these criteria, we identified several TFs, including TFAP2A, HES2, and FOSL1 (Supplementary Figure S1). Because TFAP2A is known to play a role in keratinocyte differentiation (Maytin et al, 1999; Schorle et al, 1996), we decided to focus on dissecting TFAP2A's interaction with AHR. TFAP2A is among ERGs and has an intronic AHR-bound enhancer with a high H3K27 signal (Figure 3a). AHR binding at this locus was validated by ChIP followed by qPCR (Figure 3b), establishing TFAP2A as a likely direct AHR target.

To functionally validate whether TFAP2A is a primary AHR target, clonal homozygous AHR knockout (ΔAHR) keratinocytes were generated using CRISPR/Cas9 in the immortalized N/TERT-2G keratinocyte cell line (Dickson et al, 2000). After clonal expansion of the knockout pool, a full ΔAHR clonal keratinocyte cell line was identified using PCR and subsequent Sanger sequencing. On both alleles, one nucleotide was deleted, resulting in a frameshift after 76 amino acids and an early stop codon that translates to a loss-of-function truncated AHR protein. As expected, the expression of a known AHR-target gene *CYP1A1* was significantly lower in ΔAHR keratinocytes than in wild-type cells, and *CYP1A1* expression in ΔAHR keratinocytes was only marginally enhanced by TCDD treatment, in contrast to that in wild-type

annotation of enhancers in C2, C3, and C4. (**e**) Significantly enriched motifs found in C2 and C3 of dynamic enhancers shown in **c**. (**f**) Band plot showing the quantification H3K27ac ChIP-sequencing signals at AHR-binding sites upon ligand treatment. (**g**) Band plot showing the quantification of AHR ChIP-sequencing signals at AHR-binding sites upon ligand treatment. AHR, aryl hydrocarbon receptor; C2, cluster 2; C3, cluster 3; C4, cluster 4; ChIP, chromatin immunoprecipitation; GO, gene ontology; min, minute; ns, sonsignificant.

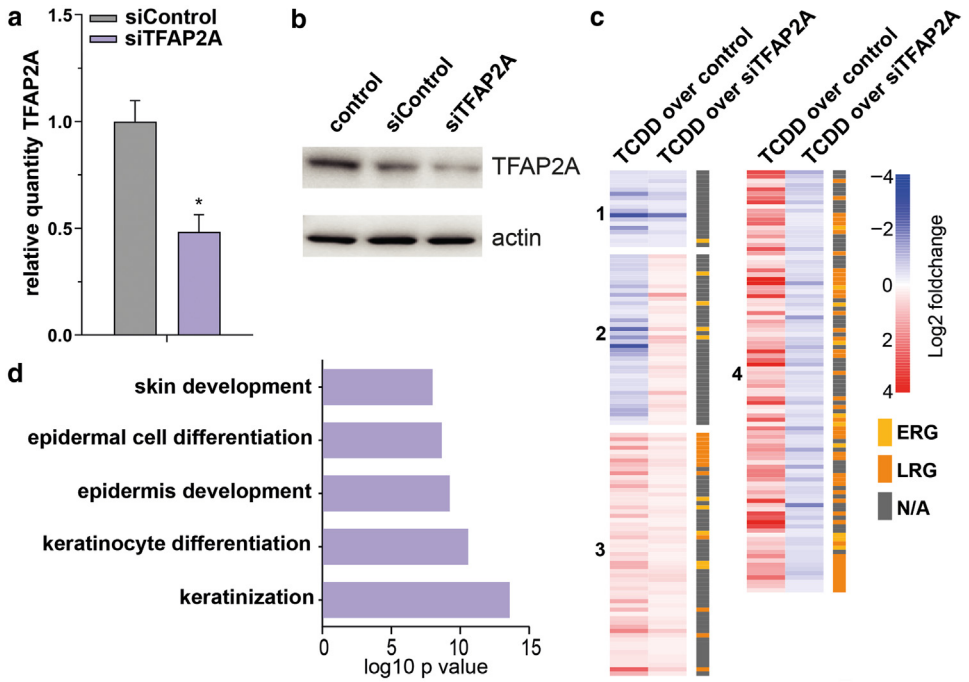

Figure 4. AHR–TFAP2A axis controls the epidermal differentiation program. (**a**) Validation of *TFAP2A* knockdown by RT-qPCR, normalized to reference gene *hARP*. Data are shown as mean ± SEM, n = 3 technical replicates, unpaired *t*-test; **P* < .05. (**b**) Western blot validation of TFAP2A knockdown. Actin was used as a loading control for the quantification of TFAP2A protein levels. (**c**) Heatmap of differentially expressed genes (*P* < .05), accompanied by ERG (yellow) or LRG (orange) nomination. Z-score was calculated on the basis of log10 (FPKM + 0.01) of each gene. (**d**) GO annotation of genes in cluster 4 of the heatmap. AHR, aryl hydrocarbon receptor; ERG, early-responsive gene; FPKM, fragments per kilobase of transcript per million mapped reads; GO, gene ontology; LRG, late-responsive gene; N/A, not available; siControl, control-targeted small interfering RNA; siTFAP2A, TFAP2A-targeted small interfering RNA.

cells (Figure 3c). Importantly, ΔAHR keratinocytes showed a loss of target gene expression, and TCDD treatment of ΔAHR keratinocytes did not increase the *TFAP2A* expression level, in contrast to the enhanced expression of *AHR* wild-type keratinocytes (Figure 3d), which is in line with our notion that *TFAP2A* is indeed an AHR direct target gene.

AHR–TFAP2A axis controls the epidermal differentiation program

Next, we investigated the contribution of TFAP2A activation in AHR-mediated keratinocyte differentiation. We knocked down *TFAP2A* in monolayer primary keratinocyte cultures using small interfering RNAs (siRNAs) (52% knockdown compared with control-targeted siRNA) (Figure 4a and b)–treated *TFAP2A*-knockdown keratinocytes with TCDD for 24 hours to activate AHR signaling, performed RNA-sequencing analysis, and detected 435 genes that were differentially expressed between TCDD-treated control-targeted siRNA and TFAP2A-targeted siRNA (Supplementary Data S4). To identify TFAP2A-mediated AHR signaling, we examined the effect of *TFAP2A* knockdown on TCDD-induced gene expression and compared them with that of the earlier identified panel of AHR-responsive genes (Figure 1d) (all clusters, 3084 DEGs in total; 1976 genes upregulated and 1108 genes downregulated). Among the 435 DEGs upon TFAP2A knockout, 214 were overlapping with the identified 3084 AHR-responsive genes. The overlapping genes were clustered according to their expression patterns (Figure 4c and Supplementary Data S4). Clusters 1 and 2 (18 and 40 genes, respectively) contain genes that are downregulated by TCDD and remain downregulated (cluster 1) or become upregulated (cluster 2) upon TCDD treatment in *TFAP2A*-knockdown condition. Clusters 3 and 4 (57 and 99 genes, respectively) contain genes that are upregulated by TCDD treatment and remain upregulated in both conditions (cluster 3) or become downregulated upon TCDD treatment in *TFAP2A*-knockdown condition (cluster 4). Because cluster 4 genes were induced by TCDD, and the induction was abolished by *TFAP2A* knockdown, these genes were marked as TFAP2A-mediated AHR-response genes. Cluster 4 was found to be enriched for LRGs (mean fold enrichment of 20.8, hypergeometric *P* = 7.11e-47), including *IVL*, several *S100* genes, and *SPRR* genes that are involved in terminal differentiation of epidermal keratinocytes. In line with this, functional annotation of the genes in cluster 4 resulted in 57 significantly enriched GO terms, such as epidermis development and keratinocyte differentiation (Figure 4d).

To investigate whether TFAP2A directly regulates these genes, we sought for the TFAP2A-binding motif near promoter and enhancers of genes in cluster 4. We found that 64 of 99 genes have a TFAP2A-binding motif at their promoter regions, whereas all 99 genes have TFAP2A motif at their enhancer regions (Supplementary Data S5). These results indicate that TFAP2A likely regulates these cluster 4 genes directly and support the notion that AHR controls keratinocyte differentiation through the activation of TFAP2A.

Finally, the importance of the identified AHR–TFAP2A axis in keratinocyte differentiation was investigated by knocking out TFAP2A using CRISPR/Cas9 on immortalized N/TERT-2G keratinocytes. Clonal homozygous TFAP2A-knockout (ΔTFAP2A) N/TERT-2G keratinocytes were

generated, grown in monolayer cultures, and treated with TCDD for up to 72 hours, similar to the conditions of the previously described AHR-activated siRNA experiment. The upregulation of the AHR-target gene *CYP1A1* by TCDD was not altered in ΔTFAP2A keratinocytes, indicating that *CYP1A1* is not regulated through TFAP2A (Figure 5a). However, differentiation-related AHR-responsive genes, for example, *IVL*, *SPRR1A/B*, *SPRR2*, and matrix metalloproteinase 1 gene *MMP1*, of which expression could be induced by TCDD in wild-type keratinocytes, were not upregulated in ΔTFAP2A keratinocytes (Figure 5b). The expression patterns of these genes upon TCDD treatment with TFAP2A depletion are consistent with those observed from the TFAP2A-targeted siRNA experiment (cluster 4) (Figure 5b) (compared with that from untreated condition, only 72-hour time point shown). Importantly, already at baseline, ΔTFAP2A keratinocytes showed significantly less expression of these genes than wild-type N/TERT-2G keratinocytes (Figure 5c), indicating that loss of TFAP2A is not adequately compensated. Consistently, low baseline expression in ΔTFAP2A keratinocytes was observed for many other epidermal differentiation genes detected by RT-qPCR, for example, *PRR9*, *DSG1*, *DSC1*, *S100A8*, *TRPV3*, and *TGM3* (Supplementary Figure S2a). Interestingly to note, expression of *AHR* was not hampered in ΔTFAP2A keratinocytes (Supplementary Figure S2b), implying that TFAP2A is not part of a self-regulating AHR signaling feedback loop. In summary, these data demonstrate that TFAP2A is an indispensable regulator in the molecular cascade of AHR-mediated keratinocyte differentiation, although it is unlikely that TFAP2A is involved in other AHR-mediated biological processes, such as xenobiotic metabolism where *CYP1A1* is a target.

ΔTFAP2A organotypic human epidermal equivalents (HEEs) were generated to examine whether TFAP2A knockout and accompanied loss of keratinocyte-differentiation gene expression give rise to morphological changes and epidermal barrier defects. Quantitative epidermal barrier properties were analyzed by electrical impedance spectroscopy (EIS) and transepidermal water loss (TEWL) (Figure 5d and Supplementary Figure S2c [for complete EIS spectrum]). ΔTFAP2A organotypic HEEs showed reduced electrical impedance, indicating functional skin barrier defects of ΔTFAP2A organotypic HEEs, which agrees with the altered keratinocyte-differentiation gene expression. Of note, we observed a statistically significant improvement in the EIS values upon AHR activation by TCDD in ΔTFAP2A organotypic HEEs, which was corroborated by a nonsignificant trend of reduction in TEWL. The loss of TFAP2A expression was confirmed by immunochemistry staining (Figure 5e), which coincided with altered epidermal morphology, for example, a significantly thinner viable epidermis and stratum corneum (Figure 5f) and stratum granulosum appearing to consist of fewer layers. As expected, on the basis of the epidermal morphology of the ΔTFAP2A organotypic HEEs, aberrant protein expression of a panel of important terminal differentiation proteins was detected, including IVL, FLG, HRNR, and TGM1 (Figure 5g). Treatment of ΔTFAP2A organotypic HEEs with TCDD did alleviate some of the diminished protein expression, suggesting that loss of TFAP2A can partially be alleviated by AHR activation, presumably through other AHR-induced ERGs (eg, *OVOL1* [Nair et al, 2006], fold change = 2.29 [Supplementary Data S1]) that cooperate in the terminal differentiation program.

DISCUSSION

In this study, we aimed to elucidate the signaling cascades through which the AHR exerts transcriptional regulation of terminal differentiation and skin barrier formation. We combined transcriptomic and epigenomic analyses to characterize the temporal gene regulatory events after AHR activation using keratinocytes as a model system for barrier epithelia. We identified that in a temporal distinct early response, AHR directly regulates the expression of several TFs known to be important for skin development and keratinocyte differentiation, for example, *TFAP2A* (Maytin et al, 1999; Mazina et al, 2001; McDade et al, 2012). Studies on human and animal models indicated that *TFAP2A*, together with *IRF6*, *GRHL3*, and *TP63*, forms a core gene regulatory network because loss of any of these genes results in similar craniofacial, epidermal, and limb development defects (Kousa and Schutte, 2016). We found that TFAP2A directly enhances epidermal differentiation as a secondary response to AHR activation and thereby contributes to skin barrier integrity. Low-level activation of AHR by endogenous, circulating, weak AHR agonists might drive the TFAP2A-mediated keratinocyte differentiation in vivo. As such, these findings further elucidate the molecular mechanisms of action through which AHR induces its target effects.

Among the many biological roles that AHR has been associated with in the skin, our study specifically unravels the molecular mechanism behind AHR-mediated keratinocyte differentiation. We identified distinct early and late responses upon AHR activation where TFs activated during the early response such as TFAP2A regulate keratinocyte-differentiation genes in the late response. In addition, we demonstrate that AHR activation leads to enhancer dynamics that distinguish direct targets from secondary effects. The AHR:AHR nuclear transporter—binding motif was significantly enriched in enhancers that were pre-established open chromatin regions with visible H3K27ac signals already before the treatment started. Thus, instead of establishing de novo enhancers, such as pioneer TFs (eg, TP63) that orchestrate the cell type—specific enhancer landscape (Kouwenhoven et al, 2015; Qu et al, 2018), AHR seems to exploit a prespecified landscape of targets. This enables a swift response toward external threats through regulation of canonical pathways such as the cytochrome P450 pathway and MAPK (Whitlock, 1999). Enhancers that showed dynamic H3K27ac signals at later time points were located near genes involved in keratinocyte differentiation, of which activation represents secondary effects of AHR activation. Interestingly, many of these genes are considered antimicrobial peptides, consistent with our and others' recent findings that AHR activation in keratinocytes induces antimicrobial peptide expression (Smits et al, 2020; Uberoi et al, 2021). It is important to note that AHR direct targets that have AHR:AHR nuclear transporter motif—containing enhancers nearby, for example, *CYP1A1*, are not all regulated by TFs such as TFAP2A, indicating the specificity of AHR action in different biological processes. In addition, immune

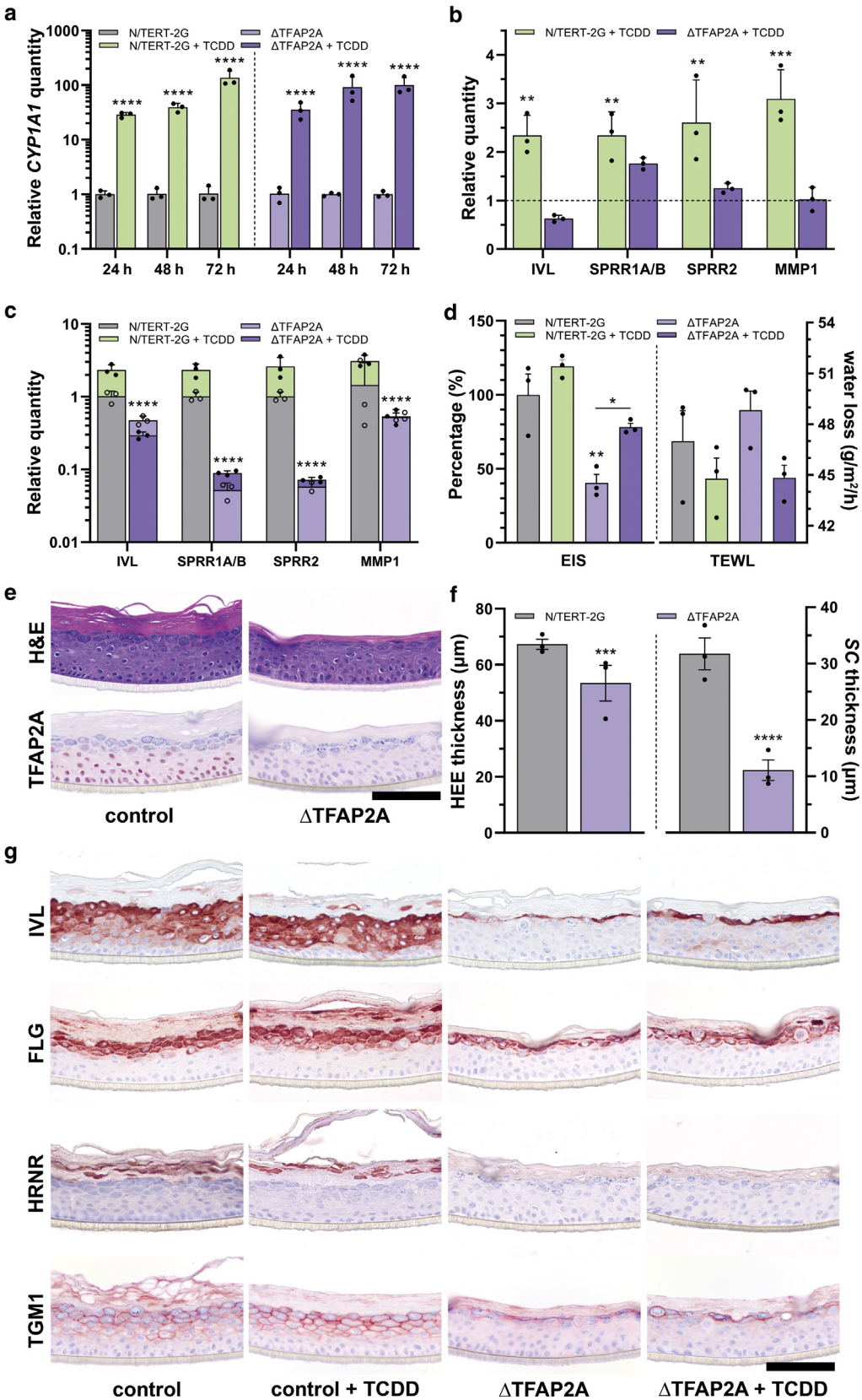

Figure 5. AHR–TFAP2A axis in keratinocyte differentiation and function. (**a**) Monolayer N/TERT-2G and ΔTFAP2A were treated with TCDD for up to 72 h, and AHR activation was validated by *CYP1A1* RT-qPCR. Data are shown as mean ± SEM, n = 3 technical replicates, 2-way ANOVA. (**b**) RT-qPCR analysis of several genes from cluster 4 (Figure 4c) displays AHR-dependent induction in the N/TERT-2G keratinocytes but not in ΔTFAP2A keratinocytes. Data are compared with those of their respective untreated condition and shown as mean ± SEM, n = 3 technical replicates, 2-way ANOVA. (**c**) In addition, RT-qPCR analysis shows a significant reduction of basal gene expression in ΔTFAP2A keratinocytes regardless of AHR activation. TCDD treatment data (closed circles) are shown superimposed on untreated data (open circles). Data are depicted as mean ± SEM, n = 3 technical replicates. (**d**) Functional skin barrier analysis EIS and TEWL

system–related functions appear to be associated with both pre-established and dynamic chromatin regions, suggesting that different immune genes are either induced or repressed at different time points upon AHR activation (Supplementary Data S2). This intriguing complexity and in the temporal cooperation between different immune pathways in response to environmental threats is subject to future research and may shed further light on the Janus-faced role of AHR (Haarmann-Stemmann et al, 2015).

Unlike AHR-binding profiles in cancer cell lines that contain thousands of AHR-binding sites (including TFAP2A) (Lo and Matthews, 2012), our AHR ChIP sequencing in keratinocytes yielded only 57 AHR-binding site, probably owing to the transient binding nature of AHR upon ligand activation in normal cells. The validation of several sites by ChIP RT-qPCR strengthens our confidence that these are genuine AHR-bound regions having biological relevance. The use of cancer cell lines (eg, HaCaT keratinocytes) in this field of research may thus overestimate the number of target genes that are actually bound by AHR under physiological conditions.

The similarity observed between TCDD and CT treatment in vitro is striking, when considering that these are on opposite sides of the health spectrum: TCDD is highly toxic, whereas CT is used as a dermatological therapy for psoriasis and atopic dermatitis (Forrester et al, 2014; Smits et al, 2020; Sorg, 2014; Tang et al, 2008; van den Bogaard Ellen et al, 2013). Previous studies reported decreased TFAP2A expression in lesional psoriasis skin and identified TFAP2A as a core TFs to regulate the psoriasis transcriptome (Rácz et al, 2011; Zolotarenko et al, 2016). Restoration of TFAP2A expression in both conditions may therefore be part of the therapeutic effect of CT. TCDD and CT both activated AHR similarly, provoking an adjective transcriptional response in keratinocytes. However, it is important to realize that the short-term effects of AHR activation in an experimental in vitro system do not take into account the ligand metabolism, degradation and elimination that would normally occur in vivo. TCDD's extreme long half-life (not being a substrate for xenobiotic metabolism) and systemic exposure have devastating chronic effects through sustained AHR activation (Panteleyev and Bickers, 2006). In contrast, CT is a highly complex mixture of many different chemicals that could counteract or compensate for the agonistic effects and is given only localized and periodically to patients with psoriasis and atopic dermatitis. This raises an interesting question on the proposed AHR ligand promiscuity at the molecular level (Denison et al, 2011). The dosage and half-life of AHR ligands and thus strength and duration of AHR activation may determine the biological effect. Whether AHR ligands are stable or rapidly metabolized or whether secondary metabolites are involved in activities independent of AHR signaling pathways requires further investigation (Heath-Pagliuso et al, 1998). In this study, timing seems to be of utmost importance, and time-course global gene expression profiling in vivo is an essential next step to evaluate AHR activation and to dissect this regulatory cascade in greater detail.

Over the years, evidence has grown that serum levels of dietary-derived or microbiota-derived components can activate the AHR in several barrier organs in vivo. For example, indole-3-carbinole can robustly activate the AHR in the intestine (Hammerschmidt-Kamper et al, 2017), whereas tryptophan metabolites can regulate AHR activation in the skin (eg, 6-formylindolo[3,2-b]carbazole [Wincent et al, 2009], kynurenine [Opitz et al, 2011], and kynurenic acid [DiNatale et al, 2010]). This implies that dietary intervention can be helpful in controlling AHR activation and thus support TFAP2A-mediated skin barrier integrity.

To conclude, our findings indicate that activation of AHR triggers a regulatory cascade mediating keratinocyte differentiation, and this cascade relies on TFs such as TFAP2A that play an intermediate but indispensable role. Our identification of the AHR–TFAP2A axis exemplifies how environmental factors can dictate the terminal differentiation process and unveil alternative routes and targets that may be hijacked to foster barrier formation and repair in the skin (and presumably other barrier organs) without the need for AHR activation per se.

MATERIALS AND METHODS

Cell culture and drug treatment

Human abdominal or breast skin was obtained from plastic surgery procedures after written, informed consent and in line with the principles and guidelines of the Declaration of Helsinki. Approval for this study by medical ethical review board was not required because only excess patient material was obtained after plastic surgery procedures. Skin biopsies were taken, and human primary keratinocytes were isolated as previously described (Tjabringa et al, 2008) and stored in liquid nitrogen until further use. Human primary keratinocytes were cultured in Keratinocyte Basal Medium (Lonza, number CC-4131) supplemented with 0.4% (vol/vol) bovine pituitary extract, 0.5 μg/ml hydrocortisone, 5 μg/ml insulin, and 10 ng/ml epidermal GF (Lonza, number CC-4131). Medium was refreshed every other day until near confluency before treatment commencement. DMSO was purchased from Merck (Darmstadt, Germany), TCDD was purchased from Accustandard, and CT was purchased from Fagron BV. Cells were treated with either DMSO (0.1% vol/vol), CT (4 μg/ml), or TCDD (10 nM). Total RNA was collected for RNA-sequencing and qPCR-based validation purposes. Chromatin was harvested for ChIP-sequencing experiments. Lysates containing

on HEEs and ΔTFAP2A organotypic HEEs display reduced electrical impedance and increased transepidermal water loss, indicating a reduced barrier functionality. Barrier functionality is improved by TCDD treatment, as EIS increases and TEWL reduces. Data are shown as mean ± SEM, n = 3 technical replicates, 1-way ANOVA. TEWL differences are not significant owing to variation in the untreated HEEs. Full EIS spectrum in Supplementary Figure S2c. (**e**) H&E staining shows the diminished HEE thickness, stratum corneum thickness, and reduced stratum granulosum. Immunohistochemistry confirms the complete loss of TFAP2A expression. (**f**) HEE and stratum corneum thickness measurements quantified and shown as mean ± SEM, n = 3 technical replicates, 2-way ANOVA. (**g**) Immunohistochemistry further indicates the reduction of IVL, FLG, HRNR, and TGM1 expression, whereas TCDD treatment marginally upregulates the expression of IVL and FLG. Bar = 100 μm. *$P < .05$, **$P < .01$, ***$P < .001$, and ****$P < .0001$. AHR, aryl hydrocarbon receptor; EIS, electrical impedance spectroscopy; h, hour; HEE, human epidermal equivalent; IVL, involucrin; MMP, matrix metalloproteinase; SC, stratum corneum; TCDD, 2,3,7,8-tetrachlorodibenzo-p-dioxin; TEWL, transepidermal water loss.

Table 2. PCR, RT-qPCR, and ChIP qPCR Primers

Gene	Usage	Forward (5′−3′)	Reverse (5′−3′)
TFAP2A	PCR	ATGGCGTGAGGTAAGGAGTG	GCTGGGCACTGTAGGTCAAT
AHR	PCR	TTCCACCAAACAATGGCTAA	AGAAGCTCTTGGCTCTCAGG
CYP1A1	RT-qPCR	CTGGAGACCTTCCGACACTCTT	GTAAAAGCCTTTCAAACTTGTGTCTCT
CYP1B1	RT-qPCR	TGGCTGCTCCTCCTCTTCAC	CCACGACCTGATCCAATTCTG
TFAP2A	RT-qPCR	TCTCCGCCATCCCTATTAAC	TGTACTTCGAGGTGGAGCTG
K2	RT-qPCR	CGCCACCTACCGCAAACT	GAAATGGTGCTGCTTGTCACA
TGM3	RT-qPCR	GGAAGGACTCTGCCACAATGTC	TGTCTGACTTCAGGTACTTCTCATACTG
hARP	RT-qPCR	CACCATTGAAATCCTGAGTGATGT	TGACCAGCCCAAAGGAGAAG
CYP1A2	ChIP qPCR	TCTCCAGGTGTCAGTTCAGG	GAGGGCACAGGAGATAGAGG
TFAP2A	ChIP qPCR	TCCGGGTAAGTTCAACACAA	AAGGGTCAGCAAGGTAAAGC
CHR11	ChIP qPCR	TTGCATATAAAGGAAACTGAAATGCT	TTACTGCCATGGGTCCGTATC
HES2	ChIP qPCR	ACCTCGGGTAACAAGACACC	AGTTTCACCTGGGGTTTTCA
FOSL1	ChIP qPCR	CATGACTCAGCCACTTCCAC	GTCTCACCGAATCGGAATTT

Abbreviations: AHR, aryl hydrocarbon receptor; ChIP, chromatin immunoprecipitation; K2, keratin 2.

proteins were harvested for western blotting purposes. No mycoplasma contaminations were found during cell culture.

N/TERT-2G culture and HEE generation

Human N/TERT keratinocyte cell line N/TERT-2G, purchased from J. Rheinwald laboratory (Harvard Medical School, Boston, MA), was cultured in Epilife medium (MEPI500CA, Thermo Fisher Scientific), complemented with human keratinocyte growth supplement (S0015, Thermo Fisher Scientific) and 1% penicillin/streptomycin (P4333, Sigma-Aldrich). HEEs were generated as previously described (Smits et al, 2017), with minor adjustments. Briefly, inert Nunc cell culture inserts (141002, Thermo Fisher Scientific) were coated with rat tail collagen (100 μg/ml, BD Biosciences) at 4 °C for 1 hour. A total of 1.5×10^5 N/TERT-2G keratinocytes (either wild-type, ΔAHR, or ΔTFAP2A keratinocytes) were seeded on the transwells in 150 μl Epilife medium (Thermo Fisher Scientific) supplemented with 1% penicillin/streptomycin (Sigma-Aldrich) in a 24-well format. After 48 hours, cultures were switched to a mixture of CnT-PR-3D medium (CELLnTEC) and DMEM medium (60:40 [v/v]) without penicillin/streptomycin for 24 hours and then cultured at the air−liquid interface for an additional 10 days. Culture medium was refreshed every other day until harvesting on day 10 of the air-exposed phase.

Transcriptional analysis by quantitative real-time PCR

Total RNA was isolated using the Favorprep total tissue RNA kit (Favorgen Biotech), according to the manufacturer's instructions. cDNA was generated after DNase treatment and used for RT-qPCR by use of the MyiQ Single-Colour Real-Time Detection System (Bio-Rad Laboratories) for quantification with Sybr Green and melting curve analysis. Primers (Table 2) were obtained from Biolegio or Merck. Target gene expression levels were normalized to the expression of human acidic RPLP0. The relative expression levels of all genes of interest were measured using the 2-ΔΔCT method (Livak and Schmittgen, 2001).

RNA sequencing and analysis pipeline

RNA sequencing was performed as described previously (Kouwenhoven et al, 2015) with the starting material of 500 ng total RNA to obtain double-strand cDNA. After purification with the MinElute Reaction Cleanup Kit (Qiagen, number 28206), 3 ng double-strand cDNA was processed for library construction using KAPA Hyper Prep Kit (Kapa Biosystems, number KK8504) according to the standard instructions except that a 15-minute USER enzyme (New England BioLab, number M5505L) incubation step was added before library amplification. The prepared libraries were quantified with the KAPA Library Quantification Kit (Kapa Biosystems, number KK4844) and then sequenced in a paired-ended manner using the NextSeq 500 (Illumina) according to standard Illumina instructions.

Sequencing reads were aligned to human genome assembly hg19 (National Center for Biotechnology Information, version 37) using STAR 2.5.0 (Dobin et al, 2013) with default options. Briefly, STAR has the option to generate in-house reference genome from the genome fastq file. In this study, hg19 genome was used to generate the in-house reference genome with the following command: STAR –runThreadN 8 –runMode genomeGenerate –genomeDir directory/ –genomeFastaFiles hg19.fa –sjdbGTFfile Homo_sapiens.GRCh37.75.gtf –sjdbOverhang 100. Then, STAR was run, and it automatically generated read counts directly. For data visualization, wigToBigWig from the UCSC genome browser tools was used to generate bigwig files and uploaded to UCSC genome browser. Genes with the mean of DESeq2-normalized counts (baseMean) > 10 were considered to be expressed. Differential gene expression (adjusted $P < .05$) and principal component analysis were performed with the R package DESeq2 using read counts per gene (Love et al, 2014). Hierarchical clustering was performed on the basis of log10 (fragments per kilobase of transcript per million mapped reads +0.01). Functional annotation of genes was performed with DAVID (Huang da et al, 2009). For the experiments containing siRNAs, read counts were generated as described earlier. Differential expression analysis was performed using R community−created R packages stringr (Wickham, 2019) and dplyr (Wickham, 2020) and the DESeq2 package with normalization on siRNA treatment (DESeq design = siRNA). Read counts from control and TCDD-treated samples at the 24-hour stimulation time point were reanalyzed in a separate DESeq2 differential expression analysis (DESeq design = treatment). Significant DEGs overlapping between both experiments (Benjamini−Hochberg adjusted $P < .05$) (Benjamini and Hochberg, 1995) were visualized in a heatmap using the ComplexHeatmap package (Gu et al, 2016). GO analysis of interesting groups was performed using clusterProfiler (Yu et al, 2012). Identification of TFs was performed as described before (Saeed et al, 2014).

ChIP sequencing and analysis pipeline

Chromatin for ChIP was prepared as previously described (Kouwenhoven et al, 2010; Qu et al, 2018). ChIP assays were performed following a standard protocol (Novakovic et al, 2016) with minor modifications. On average, 0.5 M keratinocytes were used in each ChIP. For histone mark H3K27ac, 2× ChIP reactions were pooled to prepare 1× ChIP-sequencing sample; for AHR, 4× ChIP reactions were pooled to prepare 1 ChIP-sequencing sample. Antibodies against H3K27ac (Diagenode, C15410174) and AHR (Santa Cruz Biotechnology, sc-5579) were used in each ChIP assay. Resulted DNA fragments from 4 independent ChIP assays were purified and subjected to a ChIP followed by qPCR quality check. Afterward, 5 ng DNA fragments were pooled and proceeded on with library construction using KAPA Hyper Prep Kit (Kapa Biosystems, number KK8504) according to the standard protocol. The prepared libraries were then sequenced using the NextSeq 500 (Illumina) according to standard Illumina protocols.

Sequencing reads were aligned to human genome assembly hg19 (National Center for Biotechnology Information, version 37) using BWA (Li and Durbin, 2009). Mapped reads were filtered for quality, and duplicates were removed for further analysis. In addition. The bamCoverage script was used to generate and normalize bigwig files with the FPKM (fragments of the transcript per kilobase per million mapped reads) formula. The peak calling was performed with the MACS2 (Zhang et al, 2008) against a reference input sample from the same cell line with standard settings and a q-value of 0.05. Only peaks with a $P <$ 10e-5 were used for differential analysis with MAnorm (Shao et al, 2012). Association of peaks to genes and associated GO annotation were performed with GREAT (McLean et al, 2010), with the single nearest gene within 1 Mb association rule. *P*-values were computed with a hypergeometric distribution with false discovery rate correction. k-means clustering and heat map and band plot generation were carried out with a Python package fluff (Georgiou and van Heeringen, 2016). HOMER (http://homer.salk.edu/homer/motif/) was used for motif scan against corresponding background sequences. One thing that needs to be mentioned is that we overlapped dynamic enhancers with published DNAse I–hypersensitivity sites to narrow down regions for motif scan.

Assay for Transposase-Accessible Chromatin using sequencing and motif analysis

Assay for Transposase-Accessible Chromatin using sequencing dataset (GSE123711) was downloaded and used for motif enrichment analysis as described before (Qu et al, 2019). Briefly, Assay for Transposase-Accessible Chromatin using sequencing peaks within TSS-1 Kb to TSS+0.5 Kb were defined as promoter regions, whereas Assay for Transposase-Accessible Chromatin using sequencing peaks TSS-1 Mb to TSS+1 Mb were defined as enhancer regions. Differential motif analysis and TFAP2A motif scan within promoter regions and enhancer regions were separately performed using HOMER tool using default parameters (http://homer.salk.edu/homer/motif/).

siRNA knockdown

Human primary keratinocytes were grown to 10–15% confluency before 500 nM of Accell human SMARTpool gene targeting or nontargeting siRNA (Dharmacon) was added for 48 hours. Culture medium was subsequently refreshed and supplemented with siRNA for another 48 hours. Keratinocyte were thereafter allowed to differentiate for 24 hours in the presence of TCDD and were harvested for transcriptional analysis and western blotting as described earlier. siRNA SMARTpools include Accell Human TFAP2A (7020) SMARTpool (number E-006348-00), and Accell non-targeting Control Pool (number D-001910-10).

Single-guide RNA design, single-strand donor oligonucleotide, and synthetic Cas9

Synthetic single-guide RNAs to knockout *AHR* and *TFAP2A* gene and purified Edit-R Cas9 nuclease protein (number CAS11200) were bought from Invitrogen and IDT Technologies, respectively. Table 3 provides the details on the single-guide RNAs used.

Electroporation of ribonucleoprotein complexes and analysis of editing efficiency

N/TERT-2G keratinocytes were electroporated using the NEON transfection system 10 μL kit (Thermo Fisher Scientific). N/TERT-2G keratinocytes were detached from culture plastic and washed twice with Dubellco PBS (without calcium and magnesium) as described earlier. Meanwhile, per electroporation condition, synthetic single-guide RNA (300 ng) and Cas9 (1.5 μg) were incubated with 5 μl resuspension buffer R for 20 minutes before adding 1 × 10^5 N/TERT-2G keratinocytes. After mixing the cell suspension, the cells were electroporated using 1 pulse of 1700 V for a duration of 20 ms before immediate seeding in a prewarmed 6-well plate. DNA was isolated using the QIAamp DNA blood mini kit (51106, Qiagen) according to the manufacturer's instructions after a couple of days, and CRISPR/Cas9-induced editing efficiency was analyzed by PCR and separation of amplicon on 2% agarose gel containing 1:10,000 GelRed nucleic acid gel stain (41003, Biotium). Amplicons were purified by MinElute Gel extraction kit (28606, Qiagen) using the manufacturer's instructions and Sanger sequenced to assess editing efficiency. Sanger-sequencing reads were analyzed using the Inference of CRISPR edits webtool (ice.synthego.com, version 3, Synthego Corporation). Table 4 provides details on the PCR primers used.

Generation of clonal ΔAHR and ΔTFAP2A N/TERT keratinocytes

N/TERT-2G keratinocyte cell pools carrying AHR or TFAP2A knockouts were diluted to seed 1 cell per well (~600 cells per 60 ml of Epilife medium, 100 μl per well) into 6 × 96 well plates and allowed to grow for 1 week before refreshing the medium. After another week of culture, cells were passaged, as described earlier, into 24-well plates, 6-well plates, T25 flasks, and T75 flasks

Table 3. Sequences of the sgRNAs

Target gene	Name	sgRNA Sequence (5′–3′)	PAM Site	Manufacturer
AHR	CRISPR980378_SGM	AAGTCGGTCTCTATGCCGCT	TGG	Invitrogen TrueGuide Synthetic gRNA
TFAP2A	CRISPR887200_SGM	GGAGTAAGGATCTTGCGACT	GGG	Invitrogen TrueGuide Synthetic gRNA
TFAP2A	CRISPR887208_SGM	TGTAGTCCCTGCGAGGATCC	AGG	Invitrogen TrueGuide Synthetic gRNA

Abbreviations: AHR, aryl hydrocarbon receptor; sgRNA, single-guide RNA.

Table 4. Regular PCR Primers for Predicted Off-Target Site Analysis

gRNA	Target	CFD[1]	Forward (5′−3′)	Reverse (5′−3′)
CRISPR887200_SGM (TFAP2A)	intergenic:CCDC141-SESTD1	0.53	GTACTGGGTCCTTCCCTTCA	AAGAGTGGGGCAGACTTTGT
	intergenic:RP11-20A20.2-AL157830.1	0.35	AAGTTAGCCTGGGCTTGTGT	GAAGCATCAAGGTCAGTTGTG
	exon:LTN1	0.32	ATCCATGTTCCCAGAGCTTC	GCCCACGCTGATTAAAAGAT
	intergenic:CHP2-PRKCB	0.31	AAAAACAGGGCTGAGAATGG	TCATAGCTCACCGCTCAAAC
	intergenic:AC092017.1-RCOR3	0.31	CACATCCCCAAAGACATGAG	GCTGACATTTCTTGGCTTGA
CRISPR887208_SGM (TFAP2A)	intergenic:ATP6V1G1P7-RPL7P45	0.75	TTCATCTACCTTTGCAGGTTGT	TCCATAGCAGAGGGGAGACT
	intron:METAP1D	0.38	GGTTAGGGCGTTGCCTATAA	GACAGCCATACTGCTTGTTGA
	intron:FAM160A1	0.31	TTTCCGTTTGTAGCAGTTGG	GCATCCTCTCTCAGCACTCA
	intergenic:RP11-91K8.2-SNORA33	0.29	TTCCACCTGCACACATTTTT	TTTCATTTGACAGGCAGAGC
	intergenic:GPRIN3-RP11-115D19.1	0.27	CTTCACCCAGTTTCCCCTAA	ACGCAAACCAAGAATGATGA
CRISPR980378_SGM (AHR)	intergenic:CTC-419K13.1-ENC1	0.29	GAGGCCACAAAACCATACAA	GGACTTGGAGAAAGCCAGAG
	intergenic:ACA64-SNX29	0.27	TGAAGGAAATGAACCAGTGC	GCCACAGCCATTTGCTTAT
	exon:AHRR/PDCD6	0.24	CACCTGACCCAGACCATCT	CAGGACAGAAAGCTTGTCCA
	intron:HECW2	0.21	GGGGGATGAAAAGCATTAAA	TTCTCTGAGTGGTGCTCAGG
	intron:AOX1	0.17	TACACCTGCCGACCAAATAA	TCAATTCTCTGCCCATCAGA

Abbreviations: AHR, aryl hydrocarbon receptor; CFD, cutting frequency determination.
[1]CFD indicates the likeliness of off-target cleavage at this particular site, based on Doench et al (2016).

subsequently before freezing them. Cell clonality was assessed by Sanger sequencing and analyzing genomic DNA at the targeted locus with the help of the Inference of CRISPR edits webtool (ice.synthego.com, version 3, Synthego).

In silico search for potential off-target effects

CRISPOR (version 4.99) (Concordet and Haeussler, 2018) was used to search for potential off-target effects dependent on the *Streptococcus pyogenes*–derived Cas9 PAM site (5′-NGG-3′), target genome (homo sapiens GRCh38/hg38), and our specific guide RNA selection. Using genomic DNA of the N/TERT-2G keratinocyte-knockout clones, the top 5 off-target sites for all guide RNAs were amplified by PCR and analyzed by Sanger sequencing to ensure that no off-target mutations occurred. Supplementary Data S6 provides the off-target analysis results, and Table 4 provides details on the PCR primers used for off-target analysis.

Epidermal barrier measurements TEWL and EIS

Epidermal barrier capabilities of epidermal equivalent cultures were studied by use of TEWL measurements and EIS. After habituation of the cultures to room temperature, TEWL was measured using the Aquaflux AF200 (Biox Systems) on day 10 of the air-exposed phase of the HEE culture. TEWL was measured in triplicate in wild-type N/TERT-2G keratinocyte and ΔTFAP2A keratinocyte HEEs. Significance was assessed using 1-way ANOVA with multiple comparisons correction (Tukey). EIS was measured using the real-time impedance detector Locsense Artemis (Locsense) with the SmartSense lid for monitoring cells in conventional transwell plates with inserts. Impedance (Ω) measurements were performed on day 10 of the air-exposed phase of the HEE culture after habituation of the HEE cultures to room temperature. EIS was measured in triplo on wild-type N/TERT-2G keratinocytes and ΔTFAP2A keratinocyte HEEs. After calibration, continuous impedance (Ω) was measured using standard settings, for example, sweeping frequency from 10 Hz to 100,000 Hz. Afterward, measured impedance was corrected with blank impedance measurements per electrode and corrected for the size of the culture insert (0.47 cm^2), resulting in impedance per cm^2 values (Ω/cm^2). Significance was assessed using 1-way ANOVA with multiple comparisons correction (Tukey).

Morphological and immunohistochemical analysis of HEEs

HEEs were fixed in 4% formalin solution for 4 hours and subsequently embedded in paraffin. A total of 6 μm sections were stained with H&E (Sigma-Aldrich) or processed for immunohistochemical analysis. Sections were blocked for 15 minutes with 5% normal goat or horse serum in PBS and subsequently incubated with the specific antibodies for 1 hour at room temperature. Next, a 30-minute incubation step with biotinylated horse anti-mouse or goat anti-rabbit (Vector Laboratories) was performed, followed by a 30-minute incubation with avidin-biotin complex (Vector Laboratories). The peroxidase activity of 3-Amino-9-ethylcarbazole was used to visualize the protein expression, and the sections were mounted using glycerol gelatin (Sigma-Aldrich). Table 5 provides details on the antibodies used for immunofluorescence, western blot, and immunohistochemistry. HEE and stratum corneum thickness were measured using Zen 3.2 (Blue Edition).

Western blotting and immunofluorescence

Cell lysates of human primary keratinocytes were collected after treatment using RIPA lysis buffer. Afterward, the lysates were sonicated (10 × 5 seconds on/off), and the samples were loaded onto SDS-PAGE gel and transferred to polyvinylidene fluoride membranes using the NuPAGE system (Life Technologies) and visualized using SuperSignal West Femto Maximum Sensitivity Substrate (Thermo Fisher Scientific, number 34095). For analysis of AHR translocation to the nucleus, direct immunofluorescence labeling was performed as described (van den Bogaard Ellen et al, 2013). Antibodies for western blotting and immunofluorescence are listed in Table 5.

Statistics and reproducibility

Dataset statistics were analyzed using the GraphPad Prism software. Differences under $P < .05$ were considered statistically significant. $P > .05$ denotes no significant; $^*P < .05$, $^{**}P < .01$, $^{***}P < .001$, and $^{****}P < .0001$. Gene expression analysis by RT-qPCR was performed in biological duplicates (at least n = 3); data are shown as mean ± SEM unless otherwise specified. Statistics was performed on dCT values using 1-way ANOVA with multiple comparison correction (Tukey). Other statistical methods used are specified in the Materials and Methods section.

Table 5. Antibodies Used in IHC and WB

Purpose	Antibody	Manufacturer and Catalog Number	Dilution
IF	Rabbit anti-AHR	Santa Cruz Biotechnology, SC-5579	1:200
IHC	Mouse anti-CYP1A1	Santa Cruz Biotechnology, SC-25304	1:25
WB/IHC	Mouse anti-TFAP2A	Invitrogen, MA1-872	WB 1:300 IHC 1:50
WB	Mouse anti-β-Actin, AC-15	Merck	1:100,000
IHC	Mouse anti-FLG	Leica Biosystems	1:100
IHC	Rabbit anti-HRNR	Sigma-Aldrich, HPA031469	1:500
IHC	Mouse anti-IVL, Mon150	van Duijnhoven et al (1992)	1:20
IHC	Rabbit anti-Ki67	Abcam, ab16667	1:50
IHC	Horse anti-mouse, biotinylated	Vector Laboratories, BA-200-1.5	1:200
IHC	Goat anti-rabbit, biotinylated	Vector Laboratories, BA-5000-1.5	1:200

Abbreviations: AHR, aryl hydrocarbon receptor; IF, immunofluorescence; IHC, immunohistochemistry; WB, western blot.

DATA AVAILABILITY STATEMENT

All raw sequencing files, including RNA-sequencing and chromatin immunoprecipitation–sequencing analyses generated in this study have been deposited in the Gene Expression Omnibus database with the accession number GSE226047 (https://0-www-ncbi-nlm-nih-gov.brum.beds.ac.uk/geo/query/acc.cgi?acc=GSE226047).

ORCIDs

Jos P. H. Smits: http://orcid.org/0000-0003-0915-8624
Jieqiong Qu: http://orcid.org/0000-0003-0915-1342
Felicitas Pardow: http://orcid.org/0000-0002-7946-6414
Noa J. M. van den Brink: http://orcid.org/0000-0002-0826-4823
Diana Rodijk-Olthuis: http://orcid.org/0000-0002-7752-6209
Ivonne M. J. J. van Vlijmen-Willems: https://orcid.org/0000-0002-3522-2573
Simon J. van Heeringen: https://orcid.org/0000-0002-0411-3219
Patrick L. J. M. Zeeuwen: http://orcid.org/0000-0002-6878-2438
Joost Schalkwijk: http://orcid.org/0000-0002-1308-1319
Huiqing Zhou: http://orcid.org/0000-0002-2434-3986
Ellen H. van den Bogaard: http://orcid.org/0000-0003-4846-0287

CONFLICT OF INTEREST

The authors state no conflict of interest.

ACKNOWLEDGMENTS

This research has been a long endeavor with many collaborative efforts on the various aspects of the experimental work and data analysis. We are grateful for all funders throughout the years: Radboud Institute for Molecular Life Science (JS and EHvdB), National Institutes of Health (ES028244), Dutch Research Council VENI-grant 91616054 (EHvdB), Chinese Scholarship Council grant 201406330059 (JQ), and LEO Foundation grant LF18068 (PLJMZ and EHvdB). We thank all members from the Departments of Dermatology, Molecular Developmental Biology, and Molecular Biology for discussion and suggestions on the project. We especially thank Chet Loh for discussion and useful input. We thank Eva Janssen-Megens, Siebe van Genesen, and Rita Bylsma for operating the Illumina analyzer. We thank the ENCODE Consortium for sharing their data and Gary H. Perdew for the critical reading of our manuscript. EhvdB is the guarantor.

AUTHOR CONTRIBUTIONS

Conceptualization: JPHS, JQ, JS, PLJMZ, HZ, EHvdB; Data Curation: JQ, FP, HZ; Formal Analysis: JPHS, JQ, FP; Funding Acquisition: EHvdB, JS, JQ, PLJMZ; Investigation: JPHS, JQ, FP, NJMvdB, SJvH, DR-O, IMJJvV-W; Methodology: JPHS, JQ, HZ, EHvdB; Project Administration: EHvdB; Resources: EHvdB, HZ, JS; Software: JQ, FP, SJvH; Supervision: HZ, EHvdB, JS; Validation: JPHS, FP, NHvdB, DR-O, IMJJvV-W; Visualization: JPHS, JQ; Writing – Original Draft Preparation: JPHS, JQ, FP; Writing – Review and Editing: JPHS, JQ, FP, HZ, EHvdB

SUPPLEMENTARY MATERIAL

Supplementary material is linked to the online version of the paper at www.jidonline.org, and at https://doi.org/10.1016/j.jid.2024.01.030.

REFERENCES

Angelova-Fischer I, Mannheimer AC, Hinder A, Ruether A, Franke A, Neubert RH, et al. Distinct barrier integrity phenotypes in filaggrin-related atopic eczema following sequential tape stripping and lipid profiling. Exp Dermatol 2011;20:351–6.

Benjamini Y, Hochberg Y. Controlling the false discovery rate: a practical and powerful approach to multiple testing. J R Stat Soc B 1995;57:289–300.

Candi E, Cipollone R, Rivetti di Val Cervo P, Gonfloni S, Melino G, Knight R. p63 in epithelial development. Cell Mol Life Sci 2008;65:3126–33.

Concordet JP, Haeussler M. CRISPOR: intuitive guide selection for CRISPR/Cas9 genome editing experiments and screens. Nucleic Acids Res 2018;46:W242–5.

Denison MS, Nagy SR. Activation of the aryl hydrocarbon receptor by structurally diverse exogenous and endogenous chemicals. Annu Rev Pharmacol Toxicol 2003;43:309–34.

Denison MS, Soshilov AA, He G, DeGroot DE, Zhao B. Exactly the same but different: promiscuity and diversity in the molecular mechanisms of action of the aryl hydrocarbon (dioxin) receptor. Toxicol Sci 2011;124:1–22.

Di Meglio P, Duarte JH, Ahlfors H, Owens ND, Li Y, Villanova F, et al. Activation of the aryl hydrocarbon receptor dampens the severity of inflammatory skin conditions. Immunity 2014;40:989–1001.

Dickson MA, Hahn WC, Ino Y, Ronfard V, Wu JY, Weinberg RA, et al. Human keratinocytes that express hTERT and also bypass a p16(INK4a)-enforced mechanism that limits life span become immortal yet retain normal growth and differentiation characteristics. Mol Cell Biol 2000;20:1436–47.

DiNatale BC, Murray IA, Schroeder JC, Flaveny CA, Lahoti TS, Laurenzana EM, et al. Kynurenic acid is a potent endogenous aryl hydrocarbon receptor ligand that synergistically induces interleukin-6 in the presence of inflammatory signaling. Toxicol Sci 2010;115:89–97.

Dobin A, Davis CA, Schlesinger F, Drenkow J, Zaleski C, Jha S, et al. STAR: ultrafast universal RNA-seq aligner. Bioinformatics 2013;29:15–21.

Doench JG, Fusi N, Sullender M, Hegde M, Vaimberg EW, Donovan KF, et al. Optimized sgRNA design to maximize activity and minimize off-target effects of CRISPR-Cas9. Nat Biotechnol 2016;34:184–91.

Eckert RL, Adhikary G, Young CA, Jans R, Crish JF, Xu W, et al. AP1 transcription factors in epidermal differentiation and skin cancer. J Skin Cancer 2013;2013:537028.

Esser C, Bargen I, Weighardt H, Haarmann-Stemmann T, Krutmann J. Functions of the aryl hydrocarbon receptor in the skin. Semin Immunopathol 2013;35:677–91.

Forrester AR, Elias MS, Woodward EL, Graham M, Williams FM, Reynolds NJ. Induction of a chloracne phenotype in an epidermal equivalent model by 2, 3, 7, 8-tetrachlorodibenzo-p-dioxin (TCDD) is dependent on aryl hydrocarbon receptor activation and is not reproduced by aryl hydrocarbon receptor knock down. J Dermatol Sci 2014;73:10–22.

Freinkel RK, Woodley DT. The biology of the skin. Boca Raton, FL: CRC Press; 2001.

Fritsche E, Schäfer C, Calles C, Bernsmann T, Bernshausen T, Wurm M, et al. Lightening up the UV response by identification of the arylhydrocarbon receptor as a cytoplasmatic target for ultraviolet B radiation. Proc Natl Acad Sci USA 2007;104:8851–6.

Furue M, Tsuji G, Mitoma C, Nakahara T, Chiba T, Morino-Koga S, et al. Gene regulation of filaggrin and other skin barrier proteins via aryl hydrocarbon receptor. J Dermatol Sci 2015;80:83–8.

Georgiou G, van Heeringen SJ. fluff: exploratory analysis and visualization of high-throughput sequencing data. PeerJ 2016;4:e2209.

Gu Z, Eils R, Schlesner M. Complex heatmaps reveal patterns and correlations in multidimensional genomic data. Bioinformatics 2016;32:2847–9.

Haarmann-Stemmann T, Esser C, Krutmann J. The Janus-faced role of aryl hydrocarbon receptor signaling in the skin: consequences for prevention and treatment of skin disorders. J Invest Dermatol 2015;135:2572–6.

Hammerschmidt-Kamper C, Biljes D, Merches K, Steiner I, Daldrup T, Bol-Schoenmakers M, et al. Indole-3-carbinol, a plant nutrient and AhR-ligand precursor, supports oral tolerance against OVA and improves peanut allergy symptoms in mice. PLoS One 2017;12:e0180321.

Heath-Pagliuso S, Rogers WJ, Tullis K, Seidel SD, Cenijn PH, Brouwer A, et al. Activation of the Ah receptor by tryptophan and tryptophan metabolites. Biochemistry 1998;37:11508–15.

Hidaka T, Ogawa E, Kobayashi EH, Suzuki T, Funayama R, Nagashima T, et al. The aryl hydrocarbon receptor AhR links atopic dermatitis and air pollution via induction of the neurotrophic factor artemin. Nat Immunol 2017;18:64–73.

Hollingshead BD, Beischlag TV, Dinatale BC, Ramadoss P, Perdew GH. Inflammatory signaling and aryl hydrocarbon receptor mediate synergistic induction of interleukin 6 in MCF-7 cells. Cancer Res 2008;68:3609–17.

Huang da W, Sherman BT, Lempicki RA. Systematic and integrative analysis of large gene lists using David bioinformatics resources. Nat Protoc 2009;4:44–57.

Kaye J, Piryatinsky V, Birnberg T, Hingaly T, Raymond E, Kashi R, et al. Laquinimod arrests experimental autoimmune encephalomyelitis by activating the aryl hydrocarbon receptor. Proc Natl Acad Sci USA 2016;113:E6145–52.

Kousa YA, Schutte BC. Toward an orofacial gene regulatory network. Dev Dyn 2016;245:220–32.

Kouwenhoven EN, Oti M, Niehues H, van Heeringen SJ, Schalkwijk J, Stunnenberg HG, et al. Transcription factor p63 bookmarks and regulates dynamic enhancers during epidermal differentiation. EMBO Rep 2015;16:863–78.

Kouwenhoven EN, van Heeringen SJ, Tena JJ, Oti M, Dutilh BE, Alonso ME, et al. Genome-wide profiling of p63 DNA-binding sites identifies an element that regulates gene expression during limb development in the 7q21 SHFM1 locus. PLoS Genet 2010;6:e1001065.

Li H, Durbin R. Fast and accurate short read alignment with Burrows-Wheeler transform. Bioinformatics 2009;25:1754–60.

Livak KJ, Schmittgen TD. Analysis of relative gene expression data using real-time quantitative PCR and the 2(-Delta Delta C(T)) Method. Methods 2001;25:402–8.

Lo R, Matthews J. High-resolution genome-wide mapping of AHR and ARNT binding sites by ChIP-Seq. Toxicol Sci 2012;130:349–61.

Loertscher JA, Sattler CA, Allen-Hoffmann BL. 2, 3, 7, 8-tetrachlorodibenzo-p-dioxin alters the differentiation pattern of human keratinocytes in organotypic culture. Toxicol Appl Pharmacol 2001;175:121–9.

Love MI, Huber W, Anders S. Moderated estimation of fold change and dispersion for RNA-seq data with DESeq2. Genome Biol 2014;15:550.

Maytin EV, Lin JC, Krishnamurthy R, Batchvarova N, Ron D, Mitchell PJ, et al. Keratin 10 gene expression during differentiation of mouse epidermis requires transcription factors C/EBP and AP-2. Dev Biol 1999;216:164–81.

Mazina OM, Phillips MA, Williams T, Vines CA, Cherr GN, Rice RH. Redistribution of transcription factor AP-2alpha in differentiating cultured human epidermal cells. J Invest Dermatol 2001;117:864–70.

McDade SS, Henry AE, Pivato GP, Kozarewa I, Mitsopoulos C, Fenwick K, et al. Genome-wide analysis of p63 binding sites identifies AP-2 factors as co-regulators of epidermal differentiation. Nucleic Acids Res 2012;40:7190–206.

McLean CY, Bristor D, Hiller M, Clarke SL, Schaar BT, Lowe CB, et al. GREAT improves functional interpretation of cis-regulatory regions. Nat Biotechnol 2010;28:495–501.

McLean WH, Irvine AD. Old King Coal—molecular mechanisms underlying an ancient treatment for atopic eczema. J Clin Invest 2013;123:551–3.

Nair M, Teng A, Bilanchone V, Agrawal A, Li B, Dai X. Ovol1 regulates the growth arrest of embryonic epidermal progenitor cells and represses c-myc transcription. J Cell Biol 2006;173:253–64.

Nestle FO, Di Meglio P, Qin JZ, Nickoloff BJ. Skin immune sentinels in health and disease. Nat Rev Immunol 2009;9:679–91.

Nilsson B, Svedberg A, Gjorstrup P. New use of quinoline-3-carboxamide compounds; 1995. https://patents.google.com/patent/US5726183A/en. (accessed June 8, 2023).

Nomura I, Gao B, Boguniewicz M, Darst MA, Travers JB, Leung DY. Distinct patterns of gene expression in the skin lesions of atopic dermatitis and psoriasis: a gene microarray analysis. J Allergy Clin Immunol 2003;112:1195–202.

Novakovic B, Habibi E, Wang SY, Arts RJW, Davar R, Megchelenbrink W, et al. β-glucan Reverses the Epigenetic State of LPS-Induced Immunological Tolerance. Cell 2016;167:1354–68.e14.

Opitz CA, Litzenburger UM, Sahm F, Ott M, Tritschler I, Trump S, et al. An endogenous tumour-promoting ligand of the human aryl hydrocarbon receptor. Nature 2011;478:197–203.

Panteleyev AA, Bickers DR. Dioxin-induced chloracne–reconstructing the cellular and molecular mechanisms of a classic environmental disease. Exp Dermatol 2006;15:705–30.

Peppers J, Paller AS, Maeda-Chubachi T, Wu S, Robbins K, Gallagher K, et al. A phase 2, randomized dose-finding study of tapinarof (GSK2894512 cream) for the treatment of atopic dermatitis. J Am Acad Dermatol 2019;80:89–98.e3.

Pirkle JL, Wolfe WH, Patterson DG, Needham LL, Michalek JE, Miner JC, et al. Estimates of the half-life of 2,3,7,8-tetrachlorodibenzo-p-dioxin in Vietnam Veterans of Operation Ranch Hand. J Toxicol Environ Health 1989;27:165–71.

Qu J, Tanis SEJ, Smits JPH, Kouwenhoven EN, Oti M, van den Bogaard EH, et al. Mutant p63 affects epidermal cell identity through rewiring the enhancer landscape. Cell Rep 2018;25:3490–503.e4.

Qu J, Yi G, Zhou H. p63 cooperates with CTCF to modulate chromatin architecture in skin keratinocytes. Epigenetics Chromatin 2019;12:31.

Rácz E, Kurek D, Kant M, Baerveldt EM, Florencia E, Mourits S, et al. GATA3 expression is decreased in psoriasis and during epidermal regeneration; induction by narrow-band UVB and IL-4. PLoS One 2011;6:e19806.

Ramadoss P, Perdew GH. The transactivation domain of the Ah receptor is a key determinant of cellular localization and ligand-independent nucleocytoplasmic shuttling properties. Biochemistry 2005;44:11148–59.

Rannug A, Rannug U, Rosenkranz HS, Winqvist L, Westerholm R, Agurell E, et al. Certain photooxidized derivatives of tryptophan bind with very high affinity to the Ah receptor and are likely to be endogenous signal substances. J Biol Chem 1987;262:15422–7.

Rannug U, Rannug A, Sjöberg U, Li H, Westerholm R, Bergman J. Structure elucidation of two tryptophan-derived, high affinity Ah receptor ligands. Chem Biol 1995;2:841–5.

Ray SS, Swanson HI. Dioxin-induced immortalization of normal human keratinocytes and silencing of p53 and p16INK4a. J Biol Chem 2004;279:27187–93.

Rikken G, Smith KJ, van den Brink NJM, Smits JPH, Gowda K, Alnemri A, et al. Lead optimization of aryl hydrocarbon receptor ligands for treatment of inflammatory skin disorders. Biochem Pharmacol 2023;208:115400.

Rikken G, van den Brink NJM, van Vlijmen-Willems IMJJ, van Erp PEJ, Pettersson L, Smits JPH, et al. Carboxamide derivatives are potential therapeutic AHR ligands for restoring IL-4 mediated repression of epidermal differentiation proteins. Int J Mol Sci 2022;23:1773.

Rothhammer V, Quintana FJ. The aryl hydrocarbon receptor: an environmental sensor integrating immune responses in health and disease. Nat Rev Immunol 2019;19:184–97.

Saeed S, Quintin J, Kerstens HH, Rao NA, Aghajanirefah A, Matarese F, et al. Epigenetic programming of monocyte-to-macrophage differentiation and trained innate immunity. Science 2014;345:1251086.

Schorle H, Meier P, Buchert M, Jaenisch R, Mitchell PJ. Transcription factor AP-2 essential for cranial closure and craniofacial development. Nature 1996;381:235–8.

Shao Z, Zhang Y, Yuan GC, Orkin SH, Waxman DJ. MAnorm: a robust model for quantitative comparison of ChIP-Seq data sets. Genome Biol 2012;13:R16.

Smith KJ, Boyer JA, Muku GE, Murray IA, Gowda K, Desai D, et al. Editor's highlight: ah receptor activation potentiates neutrophil chemoattractant (C-X-C motif) ligand 5 expression in keratinocytes and skin. Toxicol Sci 2017b;160:83–94.

Smith SH, Jayawickreme C, Rickard DJ, Nicodeme E, Bui T, Simmons C, et al. Tapinarof is a natural AhR agonist that resolves skin inflammation in mice and humans. J Invest Dermatol 2017a;137:2110–9.

Smits JPH, Ederveen THA, Rikken G, van den Brink NJM, van Vlijmen-Willems IMJJ, Boekhorst J, et al. Targeting the cutaneous microbiota in atopic dermatitis by coal tar via AHR-dependent induction of antimicrobial peptides. J Invest Dermatol 2020;140:415–24.e10.

Smits JPH, Niehues H, Rikken G, van Vlijmen-Willems IMJJ, van de Zande GWHJF, Zeeuwen PLJM, et al. Immortalized N/TERT keratinocytes as an alternative cell source in 3D human epidermal models. Sci Rep 2017;7:11838.

Sorg O. AhR signalling and dioxin toxicity. Toxicol Lett 2014;230:225–33.

Sutter CH, Bodreddigari S, Campion C, Wible RS, Sutter TR. 2, 3, 7, 8-tetrachlorodibenzo-p-dioxin increases the expression of genes in the human epidermal differentiation complex and accelerates epidermal barrier formation. Toxicol Sci 2011;124:128–37.

Tang NJ, Liu J, Coenraads PJ, Dong L, Zhao LJ, Ma SW, et al. Expression of AhR, CYP1A1, GSTA1, c-fos and TGF-α in skin lesions from dioxin-exposed humans with chloracne. Toxicol Lett 2008;177:182–7.

Tjabringa G, Bergers M, van Rens D, de Boer R, Lamme E, Schalkwijk J. Development and validation of human psoriatic skin equivalents. Am J Pathol 2008;173:815–23.

Tsuji G, Hashimoto-Hachiya A, Kiyomatsu-Oda M, Takemura M, Ohno F, Ito T, et al. Aryl hydrocarbon receptor activation restores filaggrin expression via OVOL1 in atopic dermatitis. Cell Death Dis 2017;8:e2931.

Uberoi A, Bartow-McKenney C, Zheng Q, Flowers L, Campbell A, Knight SAB, et al. Commensal microbiota regulates skin barrier function and repair via signaling through the aryl hydrocarbon receptor. Cell Host Microbe 2021;29:1235–48.e8.

van den Bogaard EH, Bergboer JG, Vonk-Bergers M, van Vlijmen-Willems IM, Hato SV, van der Valk PG, et al. Coal tar induces AHR-dependent skin barrier repair in atopic dermatitis. J Clin Invest 2013;123:917–27.

van den Bogaard EH, Podolsky MA, Smits JP, Cui X, John C, Gowda K, et al. Genetic and pharmacological analysis identifies a physiological role for the AHR in epidermal differentiation. J Invest Dermatol 2015;135:1320–8.

van Duijnhoven JL, Schalkwijk J, Kranenborg MH, van Vlijmen-Willems IM, Groeneveld A, van Erp PE, et al. MON-150, a versatile monoclonal antibody against involucrin: characterization and applications. Arch Dermatol Res 1992;284:167–72.

Vogel CF, Chang WL, Kado S, McCulloh K, Vogel H, Wu D, et al. Transgenic overexpression of aryl hydrocarbon receptor repressor (AhRR) and AhR-mediated induction of CYP1A1, cytokines, and acute toxicity. Environ Health Perspect 2016;124:1071–83.

Wang Z, Snyder M, Kenison JE, Yang K, Lara B, Lydell E, et al. How the AHR became important in cancer: the role of chronically active AHR in cancer aggression. Int J Mol Sci 2020;22:387.

Wegner C, Stadelmann C, Pförtner R, Raymond E, Feigelson S, Alon R, et al. Laquinimod interferes with migratory capacity of T cells and reduces IL-17 levels, inflammatory demyelination and acute axonal damage in mice with experimental autoimmune encephalomyelitis. J Neuroimmunol 2010;227:133–43.

Whitlock Jr JP. Induction of cytochrome P4501A1. Annu Rev Pharmacol Toxicol 1999;39:103–25.

Wickham H. dplyr: A Grammar of Data Manipulation. https://dplyr.tidyverse.org/; 2020. (accessed June 8, 2023).

Wickham H. stringr: Simple, Consistent Wrappers for Common String Operations. https://stringr.tidyverse.org/; 2019. (accessed June 8, 2023).

Wincent E, Amini N, Luecke S, Glatt H, Bergman J, Crescenzi C, et al. The suggested physiologic aryl hydrocarbon receptor activator and cytochrome P4501 substrate 6-formylindolo[3,2-b]carbazole is present in humans. J Biol Chem 2009;284:2690–6.

Yao EF, Denison MS. DNA sequence determinants for binding of transformed Ah receptor to a dioxin-responsive enhancer. Biochemistry 1992;31:5060–7.

Yu G, Wang LG, Han Y, He QY. clusterProfiler: an R package for comparing biological themes among gene clusters. Omics 2012;16:284–7.

Zhang Y, Liu T, Meyer CA, Eeckhoute J, Johnson DS, Bernstein BE, et al. Model-based analysis of ChIP-seq (MACS). Genome Biol 2008;9:R137.

Zolotarenko A, Chekalin E, Mesentsev A, Kiseleva L, Gribanova E, Mehta R, et al. Integrated computational approach to the analysis of RNA-seq data reveals new transcriptional regulators of psoriasis. Exp Mol Med 2016;48:e268.

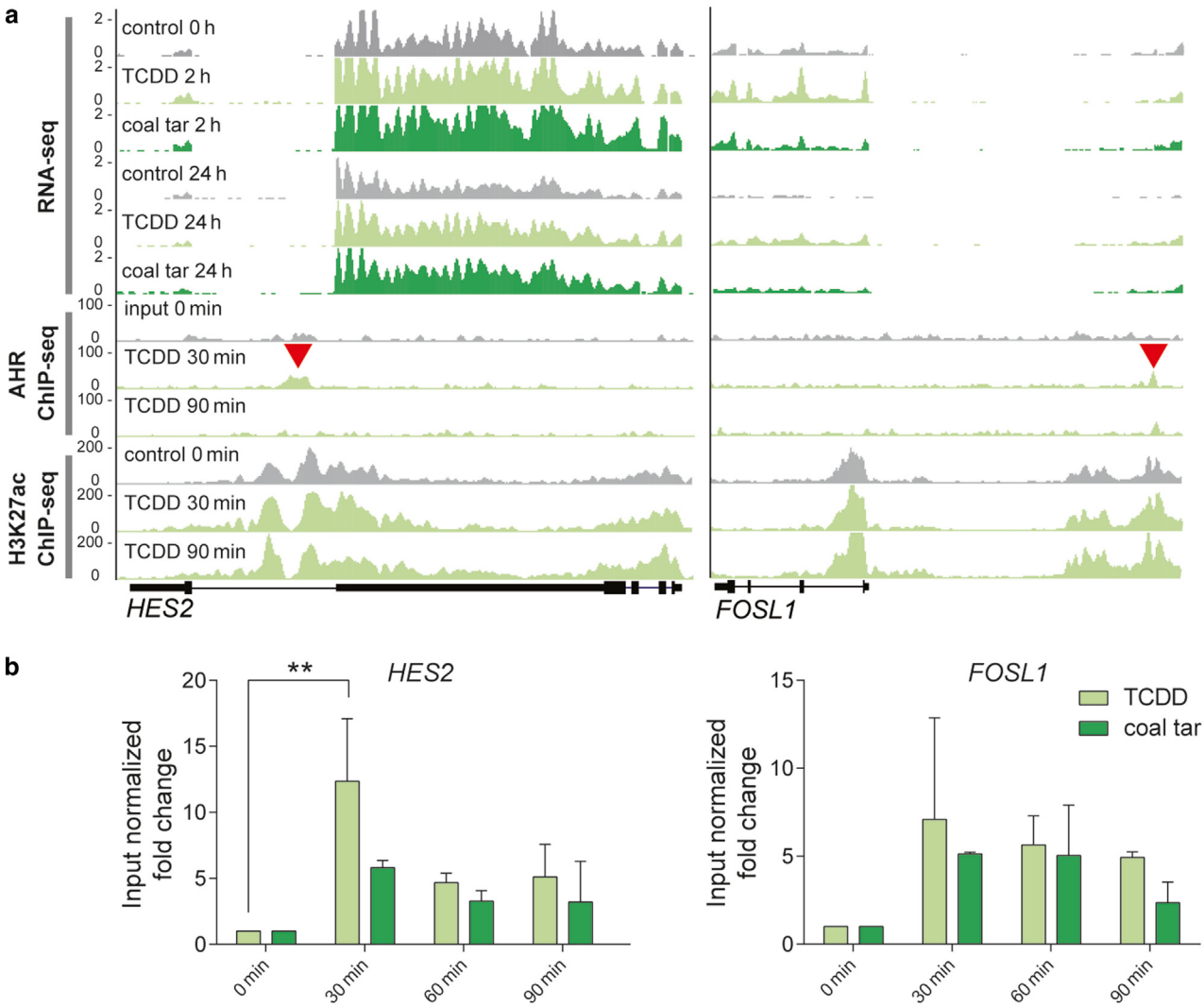

Supplementary Figure S1. AHR targets HES2 and FOSL1 in the early response to AHR ligands. (**a**) Genome browser screenshots of the *HES2* (left) and *FOSL1* (right) coding region show RNA-seq, AHR ChIP-sequencing, and H3K27ac ChIP-sequencing tracks upon treatment with coal tar and TCDD. Red arrow indicates AHR-binding site within the *HES2* and *FOSL1* loci. (**b**) AHR ChIP—RT-qPCR validation at the loci of *HES2* (left) and *FOSL1* (right) at different time point after ligand treatment. Input normalized fold change is relative to both input DNA and negative control loci (chr11). Data are shown as mean ± SEM, n = 2 technical replicates; $^{**}P < .01$. AHR, aryl hydrocarbon receptor; ChIP, chromatin immunoprecipitation; h, hour; min, minute; RNA-seq, RNA sequencing; TCDD, 2,3,7,8-tetrachlorodibenzo-p-dioxin.

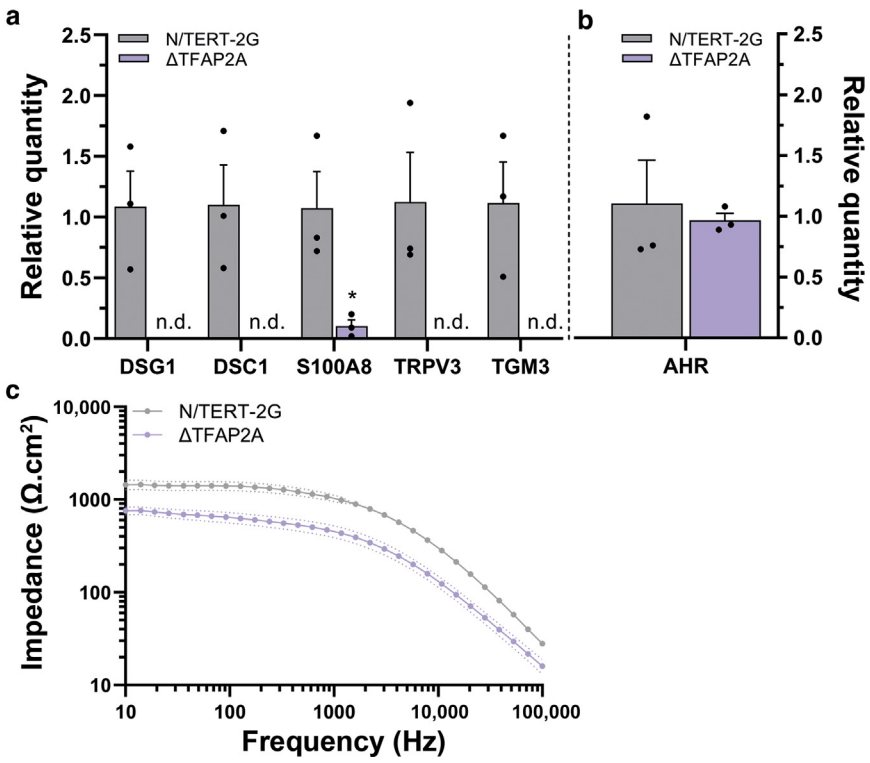

Supplementary Figure S2. Epidermal differentiation gene expression is reduced in ΔTFAP2A keratinocytes. (**a**) RT-qPCR analysis of monolayer untreated N/TERT-2G and ΔTFAP2A keratinocytes indicates that loss of TFAP2A results in severe downregulation of several epidermal differentiation genes (n.d. denotes nondetectable). Data are compared with those of N/TERT-2G keratinocytes and shown as mean ± SEM, n = 3 technical replicates, 1-way ANOVA. (**b**) *AHR* expression is not changed in monolayer ΔTFAP2A keratinocytes as shown per RT-qPCR analysis. Data are shown as mean ± SEM, n = 3 technical replicates, 1-way ANOVA. (**c**) Full EIS spectrum of HEEs and ΔTFAP2A organotypic HEEs (from Figure 5d) showing reduced electrical impedance of ΔTFAP2A organotypic HEEs. Data are shown as mean ± SEM, n = 3 technical replicates; $*P < .05$. EIS, electrical impedance spectroscopy; HEE, human epidermal equivalent.